

Ser. 1003/18
eks. 2

Utlånseksemplar



STATISTICAL REPORT

SEGMENTATION OF DATA TRACES WITH APPLICATIONS
TO DIPMETER OIL WELL MEASUREMENTS

by

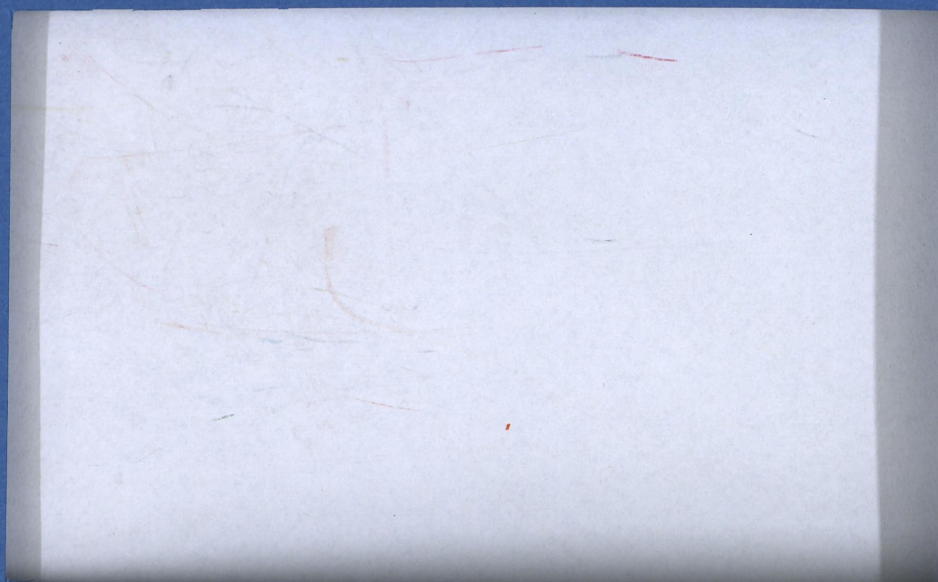
Hans Karlsen and Dag Tjøstheim

Report No 18

February 1988



Department of Mathematics
UNIVERSITY OF BERGEN
Bergen, Norway



Ser. 1003



SEGMENTATION OF DATA TRACES WITH APPLICATIONS
TO DIPMETER OIL WELL MEASUREMENTS

by

Hans Karlsen and Dag Tjøstheim

Report No 18

February 1988

Abstract:

We present a general method of automatic segmentation of a data trace. The underlying model is that of an autoregressive process with random parameters shifting according to a Markov mechanism. The data trace is segmented according to the shape and scale of its frequency distribution. The method is applied to 4-track dipmeter measurements from an unidentified drilling hole in the North Sea, and it seems to work well when the segmented dipmeter traces are inspected visually. We also do a preliminary attempt to compare with the core description and other logs which are available. At least some of the points that are of interest geologically seem to be determined more accurately by the segmented dipmeter log than by more standard logs.

1. Introduction.

Segmentation of oil well data is usually based on a number of logs such as the gamma log, the density log and the RXO and MXL logs. In addition drilling cores are used if available.

A distinct disadvantage of using these logs is that the vertical resolution is quite bad (ca. 20 cm), so that it is usually necessary to use core specimens if more detailed information is desired. However, such specimens are expensive to obtain and analyse and, as a rule, are available only a long time after the drilling.

The dipmeter log has a considerably better vertical resolution than the other logs. It is based on measuring electric conductivity by passing several (usually 4 or 8) electrodes down in the drilling hole. On modern instruments the sampling rate is 4 measurements for each centimeter leading to a resolution of ca 1 cm. We refer to Knai (1985) for a further description of its technical properties.

The dipmeter instrument is primarily constructed to measure dip of bedding planes and more specifically the structural dip resulting from tectonic stresses. The high resolution of the dipmeter has lead to suggestions that it could also provide useful information on the segmentation of the sedimentary structures. This is not entirely unproblematic since the dipmeter measures the geological properties of the drilling hole quite indirectly, and at least on older instruments there has been trouble with controlling the level of the electric current (the so-called EMEX shift, see e.g. Knai 1985). This makes the actual level of the measurements somewhat unsuitable for segmentation purposes, and perhaps due to such difficulties the literature on segmentation using the dipmeter is quite limited (see Delhomme and Serra 1984 and Kerzner 1983, however).

A statistical method of segmentation based on the main logs is given in Berteig et al (1985). See also Bølviken and Helgeland (1986) and Kerzner (1986).

To be able to exploit the dipmeter measurements in a meaningful way it seems to us that the main emphasis has to be put on characteristic features of the frequency and amplitude distribution. In Karlsen and Tjøstheim (1986) it was proposed that the dipmeter curve could be characterized by so-called autoregressive time series models, and that autoregressive parameters should be used as segmentation parameters. This approach is motivated by the use of autoregressive representation in other areas in waveform recognition (e.g. Markel and Gray 1977, Tjøstheim 1981). The modeling in the dipmeter case is made difficult by nonstationarity in level, variance as well as in frequency distribution, but the preliminary results of Karlsen and Tjøstheim (1986) indicated that the autoregressive parameters may contain useful information for segmentation purposes.

Our earlier study was hampered by the lack of a fully developed numerical segmentation algorithm pinpointing exact change points and also by the absence of core data against which our results could be tested. In the present paper we present a two-stage algorithm which nominally gives exact numerical values for the points of structural change, and we describe in more detail the relationship between autoregressive parameters and the spectral distribution (Sections 2 and 3). The algorithm is applied to an unidentified drilling hole in the North Sea for which core description as well as other logs exist, and in Section 4 we point out some common features. The evidence so far does indicate that the dipmeter trace contains information that is valuable for segmentation, and that the accuracy for some of the important change points are far better than for

the other logs. But it is also clear that it has to be used with care, and that to obtain definite conclusions geologists and petrophysicists must be involved in the interpretation, and more extensive data sets must be examined.

2. Autoregressive model fitting to dipmeter data.

For completeness and ease of reference we include in this section a short description of autoregressive model fitting to dipmeter data. Much of this material is taken from Karlsen and Tjøstheim (1986).

From a statistical modelling point of view the dipmeter trace will be considered to be a time series $\{X_t, t \in I\}$, where X_t denotes the dipmeter reading at the depth t , or the series obtained by forming differences between consecutive measurements, and where I is the observation interval. It was observed in Karlsen and Tjøstheim (1986) that in general nonstationary models are needed, but that it is reasonable to assume that the dipmeter traces are locally stationary in the sense that there are local segments where a stationarity assumption holds approximately.

The dipmeter series $\{X_t, t \in I\}$ is fitted to an autoregressive model; i.e. it is assumed that $\{X_t\}$ satisfies a difference equation

$$X_t - \mu - a_1(X_{t-1} - \mu) - \dots - a_p(X_{t-p} - \mu) = e_t, \quad (2.1)$$

where $\mu = E(X_t)$ is the expectation of X_t , where a_1, \dots, a_p are the autoregressive coefficients, and where $\{e_t\}$ is a white noise residual process with $E(e_t) = 0$ and $E(e_t e_s) = \sigma^2 \delta_{ts}$ with $\delta_{ts} = 1$ for $t = s$ and $\delta_{ts} = 0$ otherwise. Furthermore, the letter p is used to denote

the order of the series, and we use the abbreviation AR(p) to signify an autoregressive series of order p.

Alternatively (2.1) can be written

$$X_t = c + a_1 X_{t-1} + \dots + a_p X_{t-p} + e_t, \quad (2.2)$$

where $c = \mu - \sum_{i=1}^p a_i \mu$. It is seen from (2.2) that the AR assumption implies that X_t can be written as a linear combination of p previous X_t -values and a residual term e_t . The AR model is one of the main time series models, and it is described in considerable detail in numerous time series books (e.g. Box and Jenkins 1970).

Strictly speaking the dipmeter data are not time series data, and in a sense it would be more natural with a bilateral model for $\{X_t\}$ avoiding the unilateral distinction between past and present inherent in any time series model. Thus one could imagine a model of the form

$$X_t = c + \sum_{i=1}^p a_i X_{t-i} + \sum_{i=1}^q b_i X_{t+i} + e_t, \quad (2.3)$$

so that the dipmeter reading at depth t depends on the neighboring readings above and below t. However, such models are more difficult to analyse (Whittle 1954). For example least squares estimates are not consistent. Moreover, it can be shown (Whittle 1954) that bilateral schemes have an equivalent mathematical representation in terms of a one-sided autoregressive model. For reasons of mathematical and statistical convenience we will therefore use the unilateral model (2.1) in the following.

The key idea is to use the parameters μ, a_1, \dots, a_p and σ^2 appearing in (2.1) to characterize the dipmeter trace. These parameters

have certain optimality properties in a pattern recognition context although it is difficult to give them a concrete physical interpretation. Actually they depend on the sampling rate used. However, the parameters do characterize the autocorrelations or equivalently the spectral properties of $\{X_t\}$. In fact it is well known (Box and Jenkins 1970,p.56) that if $\{X_t\}$ is an AR(p) process, then the spectral density $f(\lambda)$ of $\{X_t\}$ is completely determined once the parameters a_1, \dots, a_p and σ^2 are given, since

$$f(\lambda) = \frac{2\sigma^2}{\left| 1 - \sum_{n=1}^p a_n \exp(in\lambda/\delta) \right|^2} \quad 0 \leq \lambda \leq \frac{\pi}{\delta}, \quad (2.4)$$

where δ is the sampling interval. Therefore characterizing $\{X_t\}$ by its autoregressive parameters amounts to a characterization of $\{X_t\}$ by means of its power spectral density. Moreover, since many time series can be approximated by AR(p) processes, these arguments hold approximately for a wider class of time series.

With the exception of Karlsten and Tjøstheim (1986) as far as we know autoregressive parameters have not been used before as identifiers for dipmeter data, although they have been used on a wide variety of other data such as brain waves, speech data and seismic traces.

The AR model given by (2.1) is time invariant, and it is stationary under the added constraint that the roots of the characteristic polynomial $A(z) = z^p - \sum_{i=1}^p a_i z^{p-i}$ are inside the unit circle. However, as explained in Karlsten and Tjøstheim (1986) it is clear from plots of the dipmeter traces that these data are only segmentwise stationary. This means that separate AR models must be fitted to each segment. The various segments

can be pieced together in a *timevarying* AR model defined by.

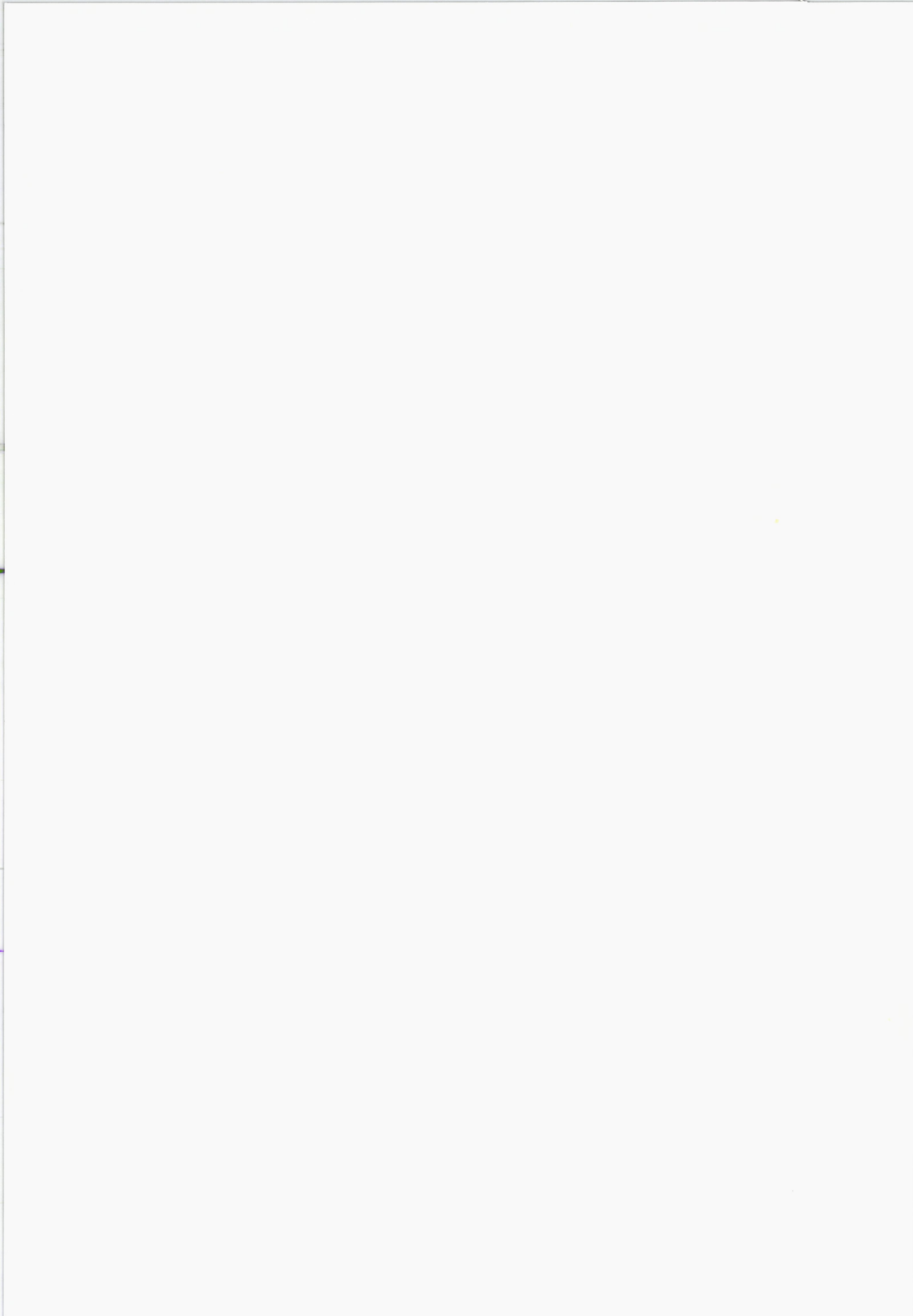
$$X_t - \mu - a_1(t)(X_{t-1} - \mu) - \dots - a_p(t)(X_{t-p} - \mu) = e_t, \quad (2.5)$$

where $\mu_t = E(X_t)$, and where $E(e_t) = 0$ and $E(e_t e_s) = \sigma_t^2 \delta_{ts}$. Here μ_t , $a_1(t), \dots, a_p(t)$ and σ_t^2 are supposed to be constant locally within each stationary segment.

As indicated in Karlsen and Tjøstheim (1986) an alternative to letting the parameters be step functions in time (or rather depth) is to let them be random processes. This results in so-called doubly stochastic processes described in Tjøstheim (1986). This apparent increase in model complexity may in fact have some simplifying effects statistically. A possibility is to let μ_t , $a_1(t), \dots, a_p(t)$ and σ_t^2 be a vector Markov chain with a finite state space, and where each state corresponds to a particular geological or petrophysical structure, which can be repeated along the borehole in a stochastic fashion according to the transition probabilities governing the Markov chain. This statistical model has been described in some detail by Tyssedal and Tjøstheim (1985), where it has been applied to economic data. In many ways a more natural application would be to dipmeter data since the segmentation mechanism inherent in the model seems more plausible in this case.

In practice the modelling via (2.5) means that a model of type (2.1) has to be fitted to each dipmeter segment. In Karlsen and Tjøstheim (1986) it was found that a low order p ($p=2,3$) gives quite a good fit to the data. Once p is determined, estimates of the parameters μ , a_1, \dots, a_p and σ^2 can be determined for example by least squares.

If a segment consists of data points X_1, \dots, X_n , then least squares



estimates for μ, a_1, \dots, a_p for this segment can be obtained by minimizing

$$F(\mu, a_1, \dots, a_p) = \sum_{t=p+1}^n (X_t - \mu - a_1(X_{t-1} - \mu) - \dots - a_p(X_{t-p} - \mu))^2. \quad (2.6)$$

This leads to the following equations for the least squares estimates

$\hat{\mu}, \hat{a}_1, \dots, \hat{a}_p$:

$$\sum_{t=p+1}^n [X_t - \hat{\mu} - \sum_{i=1}^p \hat{a}_i (X_{t-i} - \hat{\mu})] (X_{t-j} - \hat{\mu}) = 0 \quad j=1, \dots, p. \quad (2.7)$$

and

$$\sum_{t=p+1}^n [X_t - \hat{\mu} - \sum_{i=1}^p \hat{a}_i (X_{t-i} - \hat{\mu})] = 0. \quad (2.8)$$

The parameter σ^2 can then be estimated as

$$\hat{\sigma}^2 = \frac{1}{n-p-1} \sum_{t=p+1}^n \left[(X_t - \hat{\mu}) - \sum_{i=1}^p \hat{a}_i (X_{t-i} - \hat{\mu}) \right]^2. \quad (2.9)$$

Alternative estimates are maximum likelihood, Burg type and Yule-Walker estimates. In fact we have used Burg type estimates. They are similar to least squares estimates, but they are stable, i.e. the roots of the estimated characteristic polynomial are inside the unit circle, and they are quite fast. We refer to Karlsen and Tjøstheim (1986), where also a way of measuring the actual fit of an estimated AR model is described.

3. The segmentation algorithm.

We assume that the dipmeter trace can be segmented into N segments. In segment j the observations $\{X_t^j\}$ follow an $AR(p)$ model with the order p not depending on j , so that

$$X_t^j - \mu_j = \sum_{i=1}^p a_i^j (X_{t-i}^j - \mu_j) + e_t^j \quad j=1, \dots, N \quad (3.1)$$

with $E\{(e_t^j)^2\} = \sigma_j^2$ for $j=1, \dots, N$, and where we fit a separate AR model with parameters μ_j , a_1^j, \dots, a_p^j and σ_j^2 to each segment j . This corresponds to (2.5) with μ_t , $a_1(t), \dots, a_p(t)$ and σ_t^2 locally constant within each segment, and it implies that the geological structure is segmentwise homogeneous. We are currently working on models allowing continuous transitions as well (Karlsen 1986).

In Karlsen and Tjøstheim (1986) models as in (3.1) were fitted quite crudely by computing a running estimate of a_i^j (or rather $a_i(t)$ for selected time points) and approximate division points were indicated through a graphical analysis. No attempts were made to estimate the values of the coefficients within each segment or to obtain more accurate estimates of the transition points. Such estimates are clearly crucial for possible geological or petrophysical applications, and they will be provided in the present paper. The estimates are obtained by modifying an algorithm in Tyssedal and Tjøstheim (1985). It will be assumed that $\mu_j = 0$ within each segment. In fact as mentioned in Karlsen and Tjøstheim (1986) it may pay to remove μ_j by differencing of the original series. In this way at least parts of the EMEX shift will be eliminated, and therefore in the following all of our data will be assumed to be differenced.

3.1. The model.

We introduce the Markov model treated in Tjøstheim (1986) for the AR coefficients, but we stress that the algorithm as such is not dependent on the Markov assumption. It works equally well for AR models where $a_i(t)$ and σ_t^2 can only take a finite number of values a_{ji} , $j = 1, \dots, k$ and σ_j^2 , $j = 1, \dots, k_0$ in a repetitive manner, but the interpretation is different in the non-Markovian case. Related models are presented in Telknys (1986). In the doubly stochastic model (Tjøstheim 1986) we assume that the observations are generated by a stochastic process $\{X_t\}$ given by

$$X_t = \sum_{i=1}^p \theta_{ti} X_{t-i} + e_t \quad (3.2)$$

where $\{\theta_t\} = \{\theta_{t1}, \dots, \theta_{tp}\}$ is a vector Markov chain which is irreducible and aperiodic and has a finite state space consisting of k states s_1, \dots, s_k with each state s_j constituting a p -dimensional vector $s_j = [a_{j1}, \dots, a_{jp}]$. Furthermore, $\{e_t\}$ is a sequence of independent (and generally non-identical distributed) random variables with zero mean and k_0 possible values $\sigma_1^2, \dots, \sigma_{k_0}^2$ for its variance.

Alternatively $[\theta_t, \sigma_t^2]$ could be assumed to be a vector Markov process with state vectors $[s_j, \sigma_j^2]$. From the spectral formula (2.4) it is seen that spectral *shape* is determined by the autoregressive coefficients $s_j = [a_{j1}, \dots, a_{jp}]$, whereas spectral *scale* is controlled by the residual variance σ_j^2 . Each vector $[s_j, \sigma_j^2]$ $j = 1, \dots, k, k_0$ then denotes a particular state with a certain frequency structure and scaling. The idea is that such a state vector should correspond to a particular state for the geological/petrophysical properties, and that changes between Markov states should correspond to geological changes.

3.2. The algorithm.

For algorithmic purposes it is advantageous to treat the processes $\{\theta_t\}$ and $\{e_t\}$ separately. The main principles will be explained for the coefficient process $\{\theta_t\} = \{\theta_{t1}, \dots, \theta_{tp}\}$. This is assumed to be a Markov chain, and its transition probability matrix $Q = (q_{ij})$ is given by

$$q_{ij} = P(\theta_t = s_j | \theta_{t-1} = s_i) \quad i, j = 1, \dots, k \quad (3.3)$$

where $s_j = [a_{j1}, \dots, a_{jp}]$ and $s_i = [a_{i1}, \dots, a_{ip}]$ are autoregressive coefficient vectors corresponding to state i and j , respectively.

It should be noted that for an irreducible and aperiodic Markov chain with a finite state space there exists a unique vector of stationary probabilities $\pi = [\pi_1, \dots, \pi_k]$ where $\pi_i = P(\theta_t = s_i)$.

It is convenient to introduce an indicator process $\{\Delta_t\}$ indicating at each time point which state the process $\{\theta_t\}$ is in. It is defined by

$$\Delta_t = [\delta_{1t}, \delta_{2t}, \dots, \delta_{kt}] \quad (3.4)$$

where

$$\delta_{jt} = \begin{cases} 1 & \text{if } \theta_t = s_j \\ 0 & \text{otherwise} \end{cases} \quad (3.5)$$

We assume that the autoregressive order p is known in advance. One way of determining p was described in Karlsen and Tjøstheim (1986), where it was also shown how the fit can be measured afterwards. Our experience is that $p=2$ captures most of the structure of the frequency distribution after the data series has been differenced.

To start the algorithm we need initial values for k and s_1, \dots, s_k .

These are obtained by sliding and fitting an ordinary AR(p) model to segments of the data.

To be more precise, assume that data points X_1, \dots, X_n are given and consider a data interval of length $2b+1$ centered at t .

Let

$$v_t(b) = \sum_{j=t-b}^{t+b} \left(X_j - \sum_{i=1}^p a_i(t,b) X_{j-i} \right)^2 \quad (3.6)$$

for $t = b+1, b+2, \dots, n-b$, and determine estimates $\hat{a}_i(t,b)$ of the AR coefficients by minimizing $v_t(b)$. Edges can be treated by extrapolation, e.g. by putting $\hat{a}_i(t,b)$ equal to $\hat{a}_i(b+1,b)$ and $\hat{a}_i(n-b,b)$ for $t = 1, \dots, b$ and $t = n-b+1, \dots, n$, respectively. Moreover, since it can be computationally burdensome to do this routinely for every t , an alternative is to let t move in steps. In fact this is essentially the approach used in Karlsen and Tjøstheim (1986), where we had $b = 30$ and used a step length of 40.

The above estimation procedure produces p more or less smooth curves $\hat{a}_i(t,b)$, $i = 1, \dots, p$; the smoothness depending on the design parameter b and on the step length. If the model (3.2) is correct, and if the transition probabilities q_{ij} are not too large for $i \neq j$, the curves will contain typical levels corresponding to the number of states and roughly their values (cf. simulation experiments in Tyssedal and Tjøstheim 1985). Thus one can reasonably expect that quite good initial values of k and s_1, \dots, s_k can be determined when the states are reasonable far apart and do not shift too often, which is also the case of largest practical interest. It should be borne in mind that in many ways \hat{k} is the most important number coming out of the graph of $\hat{a}_i(t,b)$, $i = 1, \dots, p$, since the state vectors $s_i = [a_{i1}, \dots, a_{ip}]$,

$i = 1, \dots, k$, are reestimated later with a possibility of getting an improved estimate then.

For $1 \leq i \leq k$ and $1 \leq m \leq p$, let $A = (a_{ij})$ be the $k \times p$ matrix obtained by lumping the state vectors together. If initial values of the number of states k and of the entries (a_{im}) in the matrix A are given, then the state indicator process $\{\Delta_t\}$ defined in (3.3) and (3.4) can be estimated by minimizing a local sum of squares criterion over a window of $2c + 1$ samples, i.e. for each t choose the state $i = i(t)$ minimizing

$$R_t(c) = \sum_{j=t-c}^{t+c} \left(X_j - \sum_{m=1}^p a_{im} X_{j-m} \right)^2 \stackrel{\text{def}}{=} \sum_{j=t-c}^{t+c} e_{ji}^2 \quad (3.7)$$

for $t = p + 1 + c, \dots, n - c$. Edges can be treated as for $v_t(b)$ in (3.6).

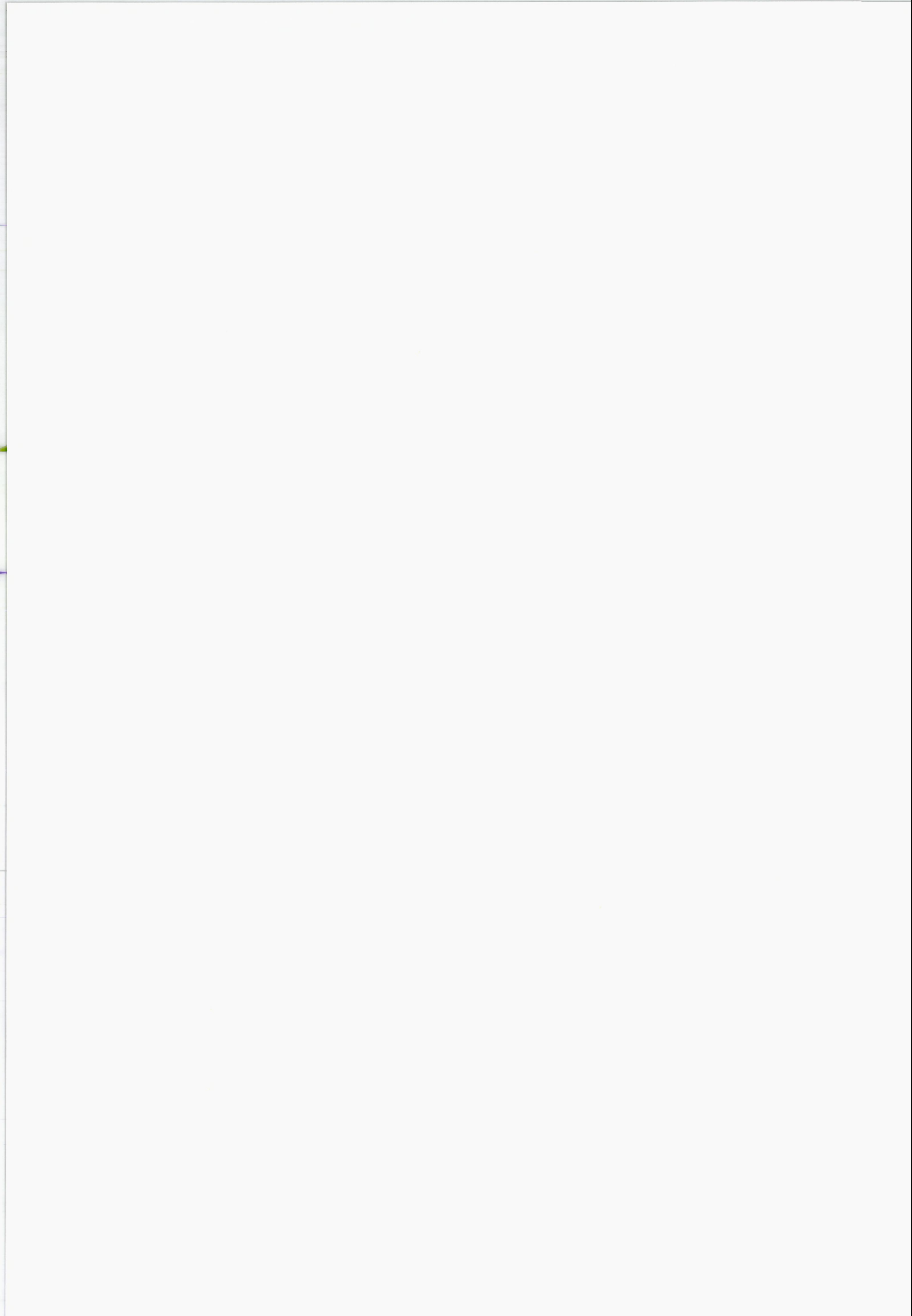
We can now reestimate $A = (a_{im})$: If k , p and $\Delta_t = [\delta_{1t}, \delta_{2t}, \dots, \delta_{kt}]$ are known, then $A = (a_{im})$ can be estimated by choosing those entries for A which minimizes the global sum of squares criterion

$$\sum_{t=p}^n \left(X_t - \sum_{m=1}^p \sum_{i=1}^k a_{im} \delta_{it} X_{t-m} \right)^2, \quad (3.8)$$

and we can then go back to (3.7) and reiterate the procedure.

The entire estimation algorithm can be summarized as follows:

1. Find input values of k and $A = (a_{im})$ from a plot of $\hat{a}_i(t, b)$, $i = 1, \dots, p$.
2. With these input values find an estimate of the state indicator process $\{\Delta_t\} = \{[\delta_{1t}, \dots, \delta_{kt}]\}$ by minimization of (3.7). This



may (Tyssedal and Tjøstheim 1985) appropriately be called the separation phase of the algorithm.

3. With this estimate of $\{\Delta_t\}$, reestimate $A = (a_{im})$ using (3.8), and if necessary go back to 2.

In Tyssedal and Tjøstheim (1985) the expression (3.7) for $R_t(c)$ was recomputed for each t . This is not necessary since it is easily shown that for i fixed the following recursion holds:

$$R_{t+1}(c) = R_t(c) + \left(X_{t+c+1} - \sum_{m=1}^p a_{im} X_{t+c+1-m} \right)^2 - \left(X_{t-c-1} - \sum_{m=1}^p a_{im} X_{t-c-1-m} \right)^2 \quad (3.9)$$

The implementation of (3.9) leads to a reduction in computer time at a factor of about 10.

From the final estimate of $\{\Delta_t\}$ it is also possible to estimate the transition probabilities $Q = (q_{ij})$ and the stationary probabilities $\pi = (\pi_i)$ as described in Tyssedal and Tjøstheim (1985). Moreover, at least approximately for slowly varying chains, standard errors of \hat{a}_{im} can be found by using the corresponding formulae for standard AR(p) processes (Box and Jenkins 1970, p.244) but with n replaced by

$n_i = \sum_{t=1}^n \delta_{it}$ which is the number of samples for which the process is in state i .

3.3. The algorithm for the residual variance.

The algorithm for segmenting the residual variance (i.e. the scale of the spectral distribution in (2.4)) has the same structure as for the autoregressive coefficients. Corresponding to the running estimate $\hat{a}_i(t,b)$ of the AR coefficient process we get a running estimate of the residual process

$$\hat{e}_t(b) = X_t - \sum_{i=1}^p \hat{a}_i(t,b) X_{t-i} \quad (3.10)$$

and a corresponding estimate of the residual variance

$$\hat{\sigma}_t^2(b) = \frac{1}{2b+1} \sum_{j=-b}^b \hat{e}_{t-j}^2(b) \quad (3.11)$$

where $\hat{\sigma}_t^2(b)$ can be extrapolated at the edges using the same technique as before.

Based on a plot of $\hat{\sigma}_t^2(b)$ we can pick the number of states k_0 , and initial values $\sigma_1^2, \dots, \sigma_{k_0}^2$ of each state. Then the transition points or the indicator process $\{\Delta_t\}$ for the σ_t^2 -process are estimated by choosing the state $i = i(t)$ which minimizes the local criterion

$$S_t(c) = \sum_{j=t-c}^{t+c} (\hat{e}_t^2 - \sigma_i^2)^2 = \sum_{j=t-c}^{t+c} (\hat{e}_t^2 - \hat{\sigma}_t^2(c))^2 + (2c+1) (\hat{\sigma}_t^2(c) - \sigma_i^2)^2 \quad (3.12)$$

where $\hat{\sigma}_t^2(c)$ is computed from (3.11) and only the last term of (3.12) is involved in the minimization.

As before we can reestimate σ_i^2 by minimizing the global sum of

squares criterion

$$\sum_t \left(\hat{\sigma}_t^2(b) - \sum_{i=1}^{k_0} \sigma_i^2 \delta_{it} \right)^2, \quad (3.13)$$

and again the algorithm can be reiterated as for the coefficient case.

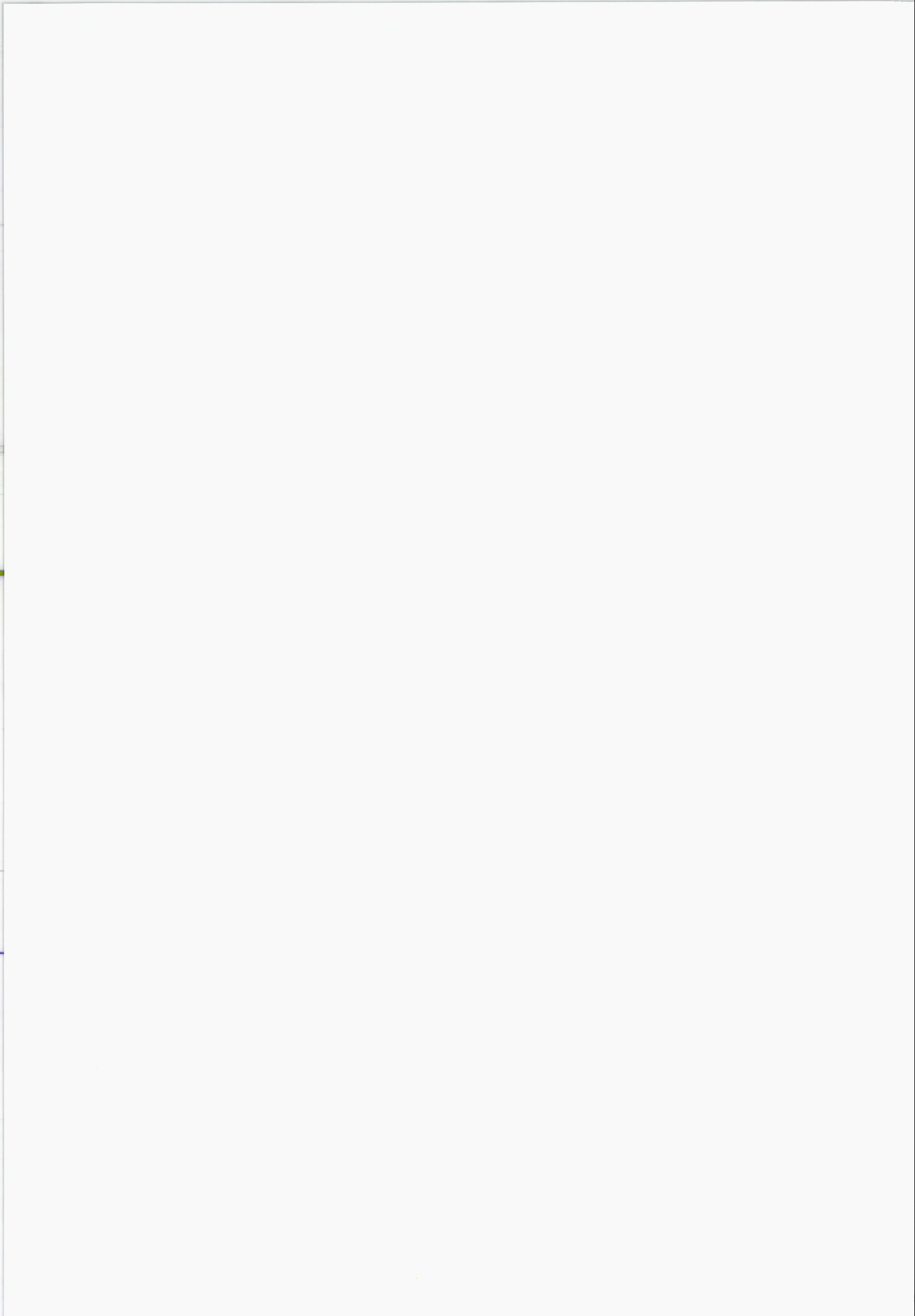
It is of course also possible to couple the two algorithms together by using step value estimates of the AR coefficients when generating $\hat{e}_t(b)$ and using estimates of the residual variance in the estimation of $a_i(t,b)$. There is a possibility that this will lead to improved estimates, and we plan to look into this at a later stage.

3.4. A more accurate determination of a single segmentation point.

Smoothing by using an average of length $2b+1$ as in formula (3.6) can lead to bias in the determination of change points, particularly if very large changes are involved from one segment to another. Since it is especially important to find an accurate value of such sharp segmentation points, we will outline a procedure for a more precise determination of a segmentation point when they are treated one at a time.

The procedure presupposes that an initial segmentation has been done according to the methods described in Sections 3.1-3.3. Let i_k , $k=1, \dots, m$ be the series of segmentation points established using the method just referred to, and assume that we want a revised estimate of i_k .

Let $\hat{a}_i(k-1)$ and $\hat{a}_i(k)$ be the estimates of $a_i(t)$ on the data stretch $i_{k-1} \leq t < i_k$ and $i_k \leq t < i_{k+1}$, respectively. The revised estimate of i_k is simply obtained by picking the s minimizing



$$\sum_{t=i_{k-1}}^s \left(X_t - \sum_{i=1}^p \hat{a}_i^{(k-1)} X_{t-i} \right)^2 + \sum_{t=s+1}^{i_k} \left(X_t - \sum_{i=1}^p \hat{a}_i^{(k)} X_{t-i} \right)^2 \quad (3.14)$$

If s is less than 10 data points from i_{k-1} or i_{k+1} , the segmentation point is removed. The estimation is carried through successively for all division points, and then the whole process can be reiterated if necessary. In a sense it would also be natural to go back to the procedure of Section 3.2 to reestimate the AR coefficients and then return to (3.14). However, in certain cases of peaked values for the parameter estimates over time we have encountered stability problems if this procedure is followed, and thus it cannot be recommended at present.

Similarly for the residual variance we reestimate a division point by picking the s minimizing

$$\sum_{t=i_{k-1}}^s (e_t^2 - \hat{\sigma}_{k-1}^2)^2 + \sum_{t=s}^{i_{k+1}} (e_t^2 - \hat{\sigma}_k^2)^2 \quad (3.15)$$

where $\hat{\sigma}_{k-1}^2$ and $\hat{\sigma}_k^2$ are the estimated values obtained by using the method of Section 3.3. Both methods will be illustrated on real data in the next section.

4. Fitting and segmentation of autoregressive models to dipmeter data from the North Sea.

In this section we undertake the actual fitting of AR models to dipmeter measurements from an unidentified drilling hole in the North Sea. Our main data set consists of measurements from a four track instrument, and a plot of the four data traces for a section of length of

approximately 20 m at a depth of 2500 m is shown in Fig. 1. It is seen from this figure that there are several common features for the traces, but that especially trace 3 deviates somewhat from the others visually.

Due to problems with the EMEX shift etc. we have found it necessary (cf. Section 3) to take differences of the data, so that the level of the measurements itself is not used in the segmentation procedure. (Possibly differencing can be avoided for the new 8-track instruments.) In the following $\{X_t\}$ will denote the differenced series; i.e. $X_t = Y_t - Y_{t-1}$ with $\{Y_t\}$ being the original measurements.

Using among other things the diagnostic checking of Karlsen and Tjøstheim (1986) it was found by a number of experiments that a second order ($p=2$ in (2.5)) AR model gives a reasonably good fit. Thus we represent $\{X_t\}$ by

$$X_t - a_1(t)X_{t-1} - a_2(t)X_{t-2} = e_t, \quad (4.1)$$

and the dipmeter trace is characterized by the three parameter functions $a_1(t)$, $a_2(t)$ and $\sigma_t^2 = E(e_t^2)$, where these are assumed to be step functions corresponding to the underlying segmentation. Running estimates of these quantities are obtained using the formulae (3.6), (3.9) and (3.10) and are displayed on Figs. 2-4 using an interval length 0.50 m and a step length of 0.10 m. These curves depict the variation in the shape of the frequency distribution $(\hat{a}_1(t,b), \hat{a}_2(t,b))$ and in the scaling of this distribution $(\hat{\sigma}_t^2(b))$. Again it is seen that there are marked similarities, but there are also considerable differences.

When we look at the residual variance plot in Fig. 4 it is seen

that there are several common peaks for all four traces. However, there are also some isolated peaks. The plots of the AR coefficients in Figs. 2 and 3 display more variation both individually and from trace to trace. A quick inspection reveals that, with the possible exception of the stretch of data from 55 - 60m, the similarity from trace to trace is most prominent in the last section of the data. Especially for the first 15 meters there seem to be considerable discrepancies.

The core description corresponding to this data section is shown in Fig. 5 together with the density and gamma log. It should be noted, however, that the core description is missing between ab. 35 - 45 m . Comparing the curves for $\hat{a}_1(t,b)$ in Fig. 2 to the density and gamma log it is seen that there are signs of a positive correlation in that high values of $\hat{a}_1(t,b)$ correspond roughly to high values for the gamma and density log and vice versa. In this context it should be remarked that Knai (1985) has only found limited evidence for correlation between these logs and the *raw* traces of the dipmeter.

In Fig. 6 the frequency distribution is shown for a trace with a high and low value for $\hat{a}_1(t,b)$, respectively. It is seen that the data segment with a high coefficient value contains a larger component of low frequency energy. This also follows theoretically from the fact that a time series with a large value for $\hat{a}_1(t,b)$ is strongly auto-correlated. Referring back to the correlation with the density log it means that a dipmeter segment coming from a higher density region tends to have a proportionally larger part of its energy in the lower frequency ranges.

We will now look at two data sections in more detail, namely 0 - 6 m and 57.5 - 70 m , and we will refine the picture given by Figs. 2-4 by using the segmentation methods of Sections 3.2 - 3.4.

4.1. The data segment 0 - 6 m .

It is seen from Fig. 6 that the core description presents an inhomogeneous and quite erratic picture for this data segment. Thus it cannot really be expected that the four dipmeter traces should all have the same structure. To illustrate the methods of Section 3 we will start by looking at trace 1 in more detail, and then discuss common features of all four traces, the density log, the gamma log and the core description.

The first stage in the segmentation methodology, is to determine initial values. From a look at the plot of $\hat{a}_1(t,b)$ and $\hat{a}_2(t,b)$ (cf. Figs. 2 and 3) four different states (levels) were identified and the initial values shown in the left hand part of Table 1 were used. Using clustering analysis would give an alternative method of determining such initial values, and this approach is currently tested.

The initial values were used as starting points for the segmentation algorithm described in Section 3.2-3.3. The algorithm was used repeatedly until we got stable values; for trace 1 shown in Table 1. In most cases of our use of the algorithm small changes occurred after the second iteration, but nevertheless on the average ca. 10 iterations were performed. For trace 1 the segmentation given in Fig. 7 was the result. In this figure are also shown the actual values a_{i1} of the segmented $\hat{a}_1(t,b)$ - coefficient. If we compare the segmentation to the visual picture of the raw trace, there appear to be some inconsistencies in particular for the 4th, 5th, 8th and 9th division point. This is thought to be due to the smoothing present in the algorithm, and to get an improved segmentation the more refined segmentation of Section 3.4 was tried. The result is given in Fig. 8. Comparing the

two figures it is seen that there are clear differences, and visually the last one seems to be the most convincing. All of the doubtful division points discussed above have been removed or shifted. Moreover, one level has been eliminated resulting in a considerably simpler picture.

It should be borne in mind that the segmentation of Fig. 8 is only based on characteristic features of the frequency distribution. Therefore it is not necessary a fault of the algorithm that the rise in amplitude at approximately 1m, say, is not separated out, because it is primarily the task of the algorithm segmenting the residual variance to detect amplitude variations (unless of course these represent frequency changes as well).

The difference in frequency content as described by the AR coefficients is quite dramatic for some of the change points, and it is certainly far beyond any statistical significance limits, since the standard errors (cf. Section 3.2) of the estimated AR coefficients for a certain state i is of the order $n_i^{-\frac{1}{2}}$ where n_i is the number of observations in this state.

The residual variance $\hat{\sigma}^2(t,b)$ was treated in the same way, and the final results based on the techniques of Section 3.4 are shown in Fig. 9. The residual process itself given by (3.9) is displayed on the same plot, and the segmentation seems quite reasonable. The rise in amplitude at about 1m is clearly captured by the segmentation, and thus it is separated out as a pure scaling effect. It is also seen that there are several other scaling effects which are independent of the frequency changes of Fig. 8.

The algorithms determine the change points with a nominal accuracy of 1cm, and the points for the AR parameters and the residual

variance corresponding to Figs. 8 and 9 have been listed in Table 2.

To get an idea about the variation from trace to trace we went through the same procedure for traces 2 - 4 , and the results are given in Figs. 10 - 15. Again the segmentation produced by the algorithm seems to correspond well to the changes that can be observed visually on the traces.

Comparing Figs. 8 - 15 it is seen that the segmentation reveals considerable differences from one trace to another, and especially trace 3 deviates from the others, which is not very surprising in view of Fig. 1. This somewhat erratic picture is perhaps what could be expected, since, as is clear from Fig. 5, the core specimens from this data section is rather inhomogeneous with quite large variations over a cross section.

However, there are also some important common features, the main ones being listed in Table 3. These features should really be correlated with the core description and the other logs to examine their possible geological significance. The most dramatic effect on the gamma and density log is the large fall in magnitude between 3.5 and 4.5 m . Corresponding to this there is a jump in grain size measured from the core specimens at approximately 4 m . It is interesting to observe that the main common feature for the frequency segmentation of Figs. 8, 10, 12 and 14 is a strong rise in AR coefficients (resulting in more energy at lower frequencies; whereas normally a fall in the neutron and density log seems to correspond to a fall in value of the AR coefficient) at 4.00 , 3.97 , 3.94 and 3.92 m , respectively. Assuming that the discontinuity is horizontal and using conventional standard errors this gives a value of 3.96 ± 0.02 m , and it seems reasonable to identify

this point with the change in the gamma and density log and the grain size just described. In fact, we understand that this point also marks the top of the oil column for this drilling hole, and the segmentation point is therefore of special significance. The main impact of the segmented dipmeter log in this case is that it allows us to pinpoint the discontinuity point much more accurately than the gamma or density log, and that this can be done without coring. Actually, virtually the same accuracy as with coring seems possible.

The most noteworthy common feature of the segmented residual plots of Figs. 9, 11, 13 and 15 is the spike at 1.61 - 1.67 , 1.58 - 1.67 and 1.54 - 1.60 m, respectively for traces 1, 2 and 4 (while trace 3 has a spike at 1.86 - 1.90 m). This could possibly correspond to the grain discontinuity observed at about this location for the cores (cf. Fig. 5). Another common feature is the increase in amplitude (residual variance) for all traces at 1.05 ± 0.03 m. Moreover trace 1 and 2 has a common descent in amplitude at 2.51 and 2.49 m, and this also corresponds very closely to a frequency change for these two traces at this location. It is an interesting task to try to interpret geologically these points and other major change points occurring more or less separately along the traces.

4.2. The data segment 57.5 - 70 m.

A corresponding analysis was done for this data segment. The drilling cores of Fig. 5 present a more homogeneous picture here, and as can be seen from Figs. 16 - 23 this is the case for the segmentation of the dipmeter traces as well. It is noted that the main features are the

same although there are many differences in detail. Again, however, trace 3 differs somewhat from the other traces. The main common features are tabulated in Table 4.

From this table and from the lower portion of Figs. 16, 18, 20 and 22 we have that there is a general alternation between regions with a large proportion of the energy at low frequencies and regions where the energy is more evenly distributed. Moreover, the main plateaus and troughs described by the AR coefficients coincide quite well.

From Figs. 17, 19, 21 and 23 and Table 4 it follows that with the exception of trace 3, the segmentation based on the residual variance has a number of common features, and there is also a high degree of consistency with the frequency segmentation for this data section with some of the change points corresponding rather closely for the individual traces.

Looking at the grain size, density log and gamma log the most dramatic effect is the change just before 70 m. This point actually marks the lower end of the oil column. It is also clearly reflected on the dipmeter log both for the frequency and residual variance segmentation and, in this case, for all four traces. For the frequency segmentation we get a division point at 69.73 ± 0.07 m, whereas the residual variance yields 69.77 ± 0.07 m, resulting in a combined estimate of 69.75 ± 0.05 . It should be noted that this point is fairly close to the end of the analysed data trace, and therefore this may have some negative effect on the accuracy.

Another noteworthy fact is that the two main higher frequency plateaus in the region 60.1-61.7 m and 65.3-66.2 m correspond roughly to the peaks of the gamma log and the density log and to the

glimmer content of the cores at these locations. This again points to a possible correlation between the gamma and density log and the segmented dipmeter log (although this is somewhat contradicted by the behavior of these logs close to the major division point at 3.96 of the first data section) with a possibility of determining division points much more accurately from the dipmeter log.

There are also a number of common features on a smaller scale for two or more of the traces, but clearly a more detailed geological analysis is needed to reach more definite conclusion.

5. Summary remarks and further research.

We have presented a general method for segmenting a data trace. The purpose of the segmentation has been to subdivide the trace into segments according to the shape and scale of the frequency distribution. The shape has been measured by the AR parameters of a second order autoregressive model, whereas the scaling is measured by the residual variance. The method seems to work well when the segmentation obtained is inspected visually for a number of raw traces. Also results from simulations (Tyssedal 1985 and Johnsen et al. 1987) seem promising. A simple simulation example is presented in Fig. 24 a) and b) showing a good correspondence between true and estimated picture.

Thus if the dipmeter trace really contains significant geological information which is reflected in the frequency or scaling properties of the curve, there should be a good possibility of exploiting this to get more accurate information on structural shift points, than is feasibly using the other logs which have a much poorer vertical resolution. We have given examples of at least two such points, which

appear to be geologically significant, and which can be more accurately determined by the dipmeter log than by the other logs, but more work remains to determine the real potential of our methods.

Further work should be concentrated on an attempt to correlate segmented parameter values more directly against geological structure. In such an analysis it will probably be necessary to use cluster and discrimination analysis. Cluster analysis could also provide input values to the segmentation algorithm, and it seems to work fairly well (Johnsen et al. 1987) in this respect. Moreover, the possibility of using recently developed image analysis techniques and robust autoregressive estimation methods (Künsch 1984) should also be explored. Finally, the new 8-track instruments may offer possibilities for using the level of the measurement in a useful way; i.e. it may not be necessary to eliminate this by differencing as for the 4-track instrument.

Acknowledgement.

This work has been supported by a grant from STATOIL. We are indebted to A. Hurst, T. Knai, T. Langeland and E. Siring for providing us with data, for documentation on the dipmeter and for useful discussions. We are grateful to G. Johnsen for carrying out the simulations leading to Fig. 24.

References.

- Berteig, V., Helgeland, J., Mohn, E., Langeland, T. and van der Wel, D. (1985). Lithofacies prediction from well data. Paper presented at SPWLA, Dallas, 17-21 June 1985.
- Box, G.E.P. and Jenkins, G.M. (1970). Time Series Analysis, Forecasting and Control. Holden Day. San Francisco.
- Bølviken, E. and Helgeland, J. (1987). Models for randomly segmented data motivated by statistical problems in oil wells, Report, Norwegian Computer Center, Oslo Norway. To appear.
- Delhomme, J.P. and Serre, O. (1984). Dipmeter-derived logs for sedimentological analysis. Preprint, Etudes et Productions Schlumberger, Montrouge.
- Johnsen, G., Karlsen, H. and Tjøstheim, D. (1987). Segmentation of data traces. Some results using simulation and clustering. In Preparation.
- Karlsen, H. (1986). Existence of moments in doubly stochastic time series models. Statistical report 16, Department of Mathematics, University of Bergen. Submitted for publication.
- Karlsen, H. and Tjøstheim, D. (1986). Fitting nonstationary autoregressive models to dipmeter data. Statistical Report 13, Department of Mathematics, University of Bergen.
- Kerzner, M.G. (1983). Formation dip determination - an artificial intelligence approach. The Log Analyst, 10-22.
- Kerzner, M.G. (1986). Image Processing in Well Log Analysis. D. Reidel, Dordrecht, Holland.
- Knai, T.A. (1985). Pattern recognition of HDT-curves and its relationship to lithofacies prediction, in Norwegian. Master thesis, University of Trondheim, NTH, Norway.
- Künsch, H. (1984). Infinitesimal robustness for autoregressive processes. Annals of Statistics, 12, 843-863.
- Markel, J.D. and Gray, A.H., Jr. (1977). Linear Prediction of Speech. Springer, New York.

- Telknys, L., editor. (1986). Detection of Changes in Random Processes. Optimization Software Inc., New York.
- Tjøstheim, D. (1981). Multidimensional discrimination techniques - theory and applications. In Identification of Seismic Sources - Earthquake or Underground Explosion. NATO. Adv. Stud. Inst. Vol. (74, E.S. Husebye and S. Mykkeltveit eds.) D. Reidel. Dordrecht, Holland, 663-694.
- Tjøstheim, D. (1986). Some doubly stochastic time series models. Journal of Time Series Analysis, 7, 51-72.
- Tyssedal, J. and Tjøstheim, D. (1985). An autoregressive model with suddenly changing parameters. Technical Report, Chr. Michelsens Institute, Dept. of Science and Technology, CMI no 822555-9, 5000 Bergen, Norway. Submitted for publication.
- Whittle, P. (1954). On stationary processes in the plane. Biometrika 41, 434-449.

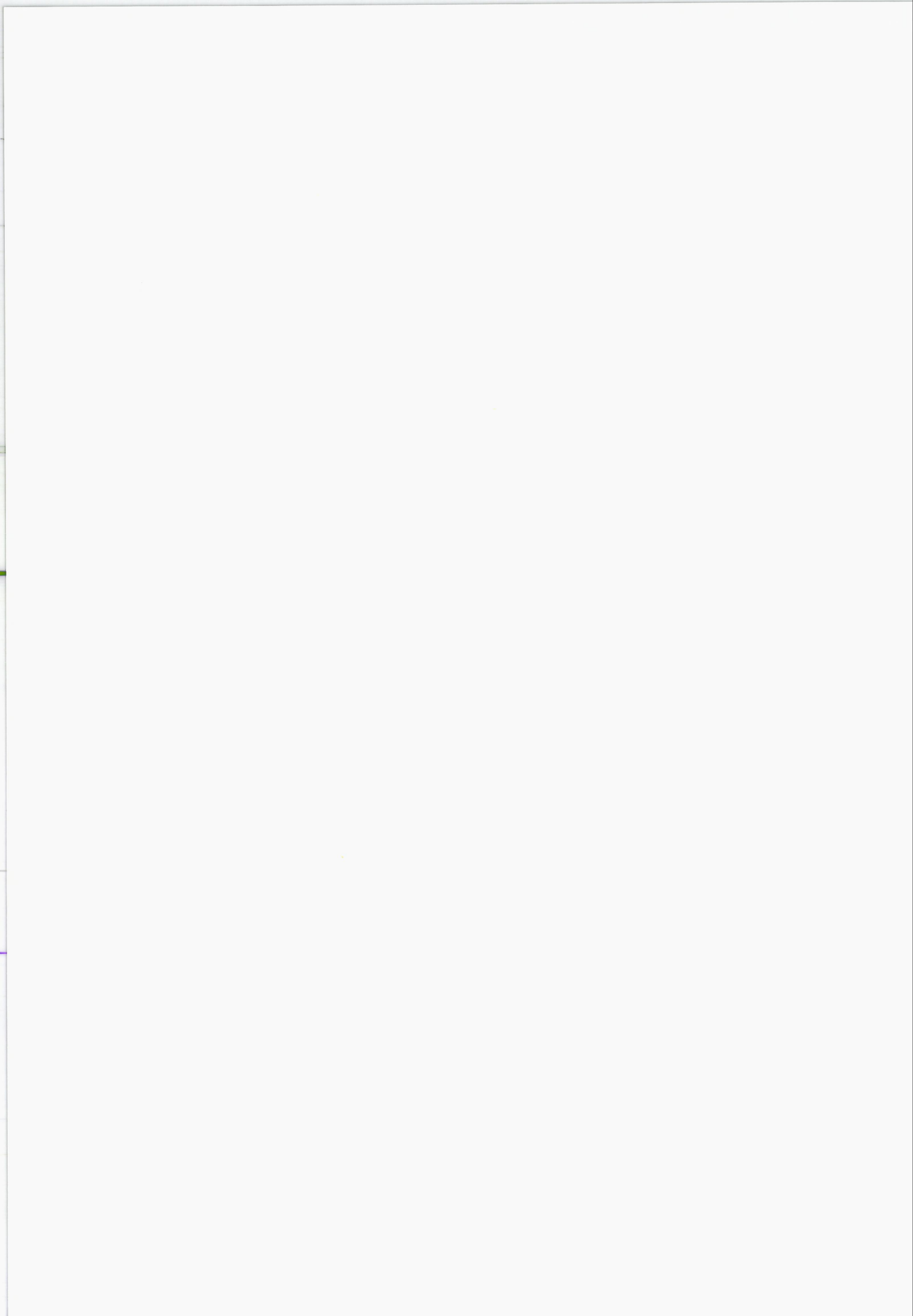


Table captions.

Table 1 : Initial values and values after 4 and 6 iterations for the first order AR coefficient, and initial values and values after 4, 8 and 10 iterations for the residual variance using the segmentation algorithm of Section 3.3 on the data section 0-6 m for trace 1.

Table 2 : Numerical values of change points for the residual variance and the AR coefficients for trace 1 corresponding to Figs. 8 and 9.

Table 3 : Some common features for the four data traces for the data section 0-6 m .

Table 4 : Some common features for the four data traces for the data section 57.5-70 m .

Table 1

AR coefficients				Residual variance				
Level	Init.v.	Iter.4	Iter.6	Level	Init.v.	Iter.4	Iter.8	Iter.10
A	1.4	1.338	1.337	A	10.0	9.70	9.70	9.70
B	1.1	1.081	1.080	B	5.0	4.42	4.51	4.51
C	0.5	0.175	0.180	C	2.5	3.47	3.58	3.58
D	0.0	-0.126	-0.126	D	1.5	1.75	1.76	1.76
				E	0.8	1.00	1.02	1.02

Table 2

AR coefficients		Residual variance	
Level	Change points	Level	Change points
A	0.0 - 1.61	D	0.0 - 1.01
B	1.62 - 1.69	C	1.01 - 1.61
A	1.70 - 2.53	A	1.61 - 1.67
C	2.54 - 4.00	D	1.67 - 2.39
A	4.00 - 4.77	B	2.39 - 2.51
C	4.77 - 5.23	D	2.51 - 2.57
A	5.24 - 6.00	E	2.57 - 3.68
		D	3.69 - 4.21
		E	4.22 - 6.00

Table 3

Trace	AR coefficients			Trace	Residual variance			
	Common changepoints				Common changepoints			
1	1.58	2.51	4.00	1	1.01	1.61	1.67	2.51
2	1.70	2.53	3.97	2	1.12	1.58	1.67	2.49
3			3.94	3	1.07			
4			3.92	4	1.10	1.54	1.60	

Table 4

AR coefficients - common changepoints

Trace	Common changepoints							
1	59.30	60.15	61.84	64.57	65.34	66.19	69.70	
2	59.11	60.07	61.84	64.50	65.26	66.22	69.78	
3	58.99	60.36	61.61	64.54	65.27	66.10	69.82	
4	59.27	60.09	61.85	64.31	65.30	66.16	69.66	

Residual variance - common changepoints

Trace	Common changepoints					
1	61.61	61.80	65.29	66.21	69.84	
2	61.67	61.98	65.40	66.29	69.77	
3	61.55	61.62			69.82	
4		61.80	65.27	66.22	69.67	

Figure captions.

Figure 1 : A data section of 70m from a 4-track dipmeter log from an unidentified drilling hole in the North Sea.

Figure 2 : Running estimates $\hat{a}_1(t,b)$ for the first order AR coefficient for all four traces.

Figure 3 : Running estimates $\hat{a}_2(t,b)$ for the second order AR coefficient for all four traces.

Figure 4 : Running estimates $\hat{\sigma}^2(t,b)$ for the residual variance for all four traces.

Figure 5 : Core description and density and gamma log.

Figure 6 : Spectral plots for a model with a high and a low set of values for the AR coefficients. In the upper part the model $X_t = 1.4X_{t-1} - 0.65X_{t-2} + e_t$ and in the lower part $X_t = 0.5X_{t-1} + 0.15X_{t-2} + e_t$.

Figure 7 : Segmentation for the data section 0-6m based on the two AR coefficients a_1 and a_2 for trace 1 using the method of Section 3.3. Only the segmented values of a_1 are shown in the lower half of the figure. The segmentation points are inserted on a plot of the differenced raw data trace in the upper part of the figure.

Figure 8 : Segmentation for the data section 0-6m based on the two AR coefficients a_1 and a_2 for trace 1 combining the methods of Sections 3.3 and 3.4. Only the values of a_1 are shown in the lower half of the figure. The segmentation points are inserted on a plot of the differenced raw data trace in the upper part of the figure.

Figure 9 : Segmentation for the data section 0-6m based on the residual variance σ^2 for trace 1 combining the methods of Sections 3.3 and 3.4. The segmented values of σ^2 are shown in the lower half of the figure. The segmentation points are inserted on a plot of the residual process as estimated from (3.9) in the upper part of the figure.

Figure 10 : Same as figure 8 for trace 2 .

Figure 11 : Same as figure 9 for trace 2 .

Figure 12 : Same as figure 8 for trace 3 .

Figure 13 : Same as figure 9 for trace 3 .

Figure 14 : Same as figure 8 for trace 4 .

Figure 15 : Same as figure 9 for trace 4 .

Figure 16 : Segmentation for the data section 57.5 - 70 m based on the two AR coefficients a_1 and a_2 for trace 1 combining the methods of Sections 3.3 and 3.4. Only the values of a_1 are shown in the lower half of the figure. The segmentation points are inserted on a plot of the differenced raw data trace in the upper part of the figure.

Figure 17 : Segmentation for the data section 57.5 - 60 m based on the residual variance σ^2 for trace 1 combining the methods of Sections 3.3 and 3.4. The segmented values of σ^2 are shown in the lower half of the figure. The segmentation points are inserted on a plot of the residual process as estimated from (3.9) in the upper part of the figure.

Figure 18 : Same as figure 16 for trace 2 .

Figure 19 : Same as figure 17 for trace 2 .

Figure 20 : Same as figure 16 for trace 3 .

Figure 21 : Same as figure 17 for trace 3 .

Figure 22 : Same as figure 16 for trace 4 .

Figure 23 : Same as figure 17 for trace 4 .

Figure 24 : a) True values of the AR coefficient a_1 and corresponding segmentation.
b) Estimated values of the AR coefficient a_1 and corresponding segmentation.

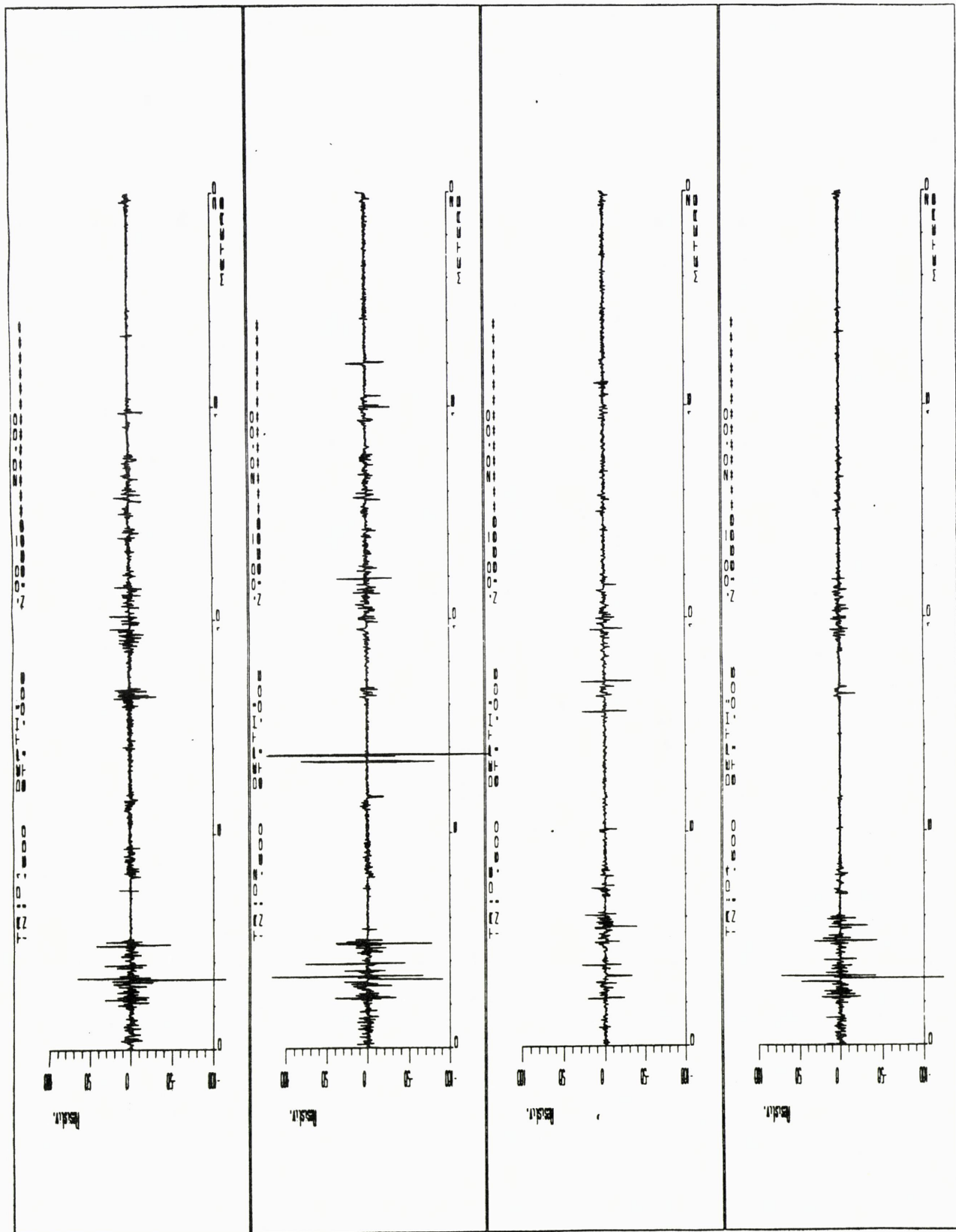


Fig. 1

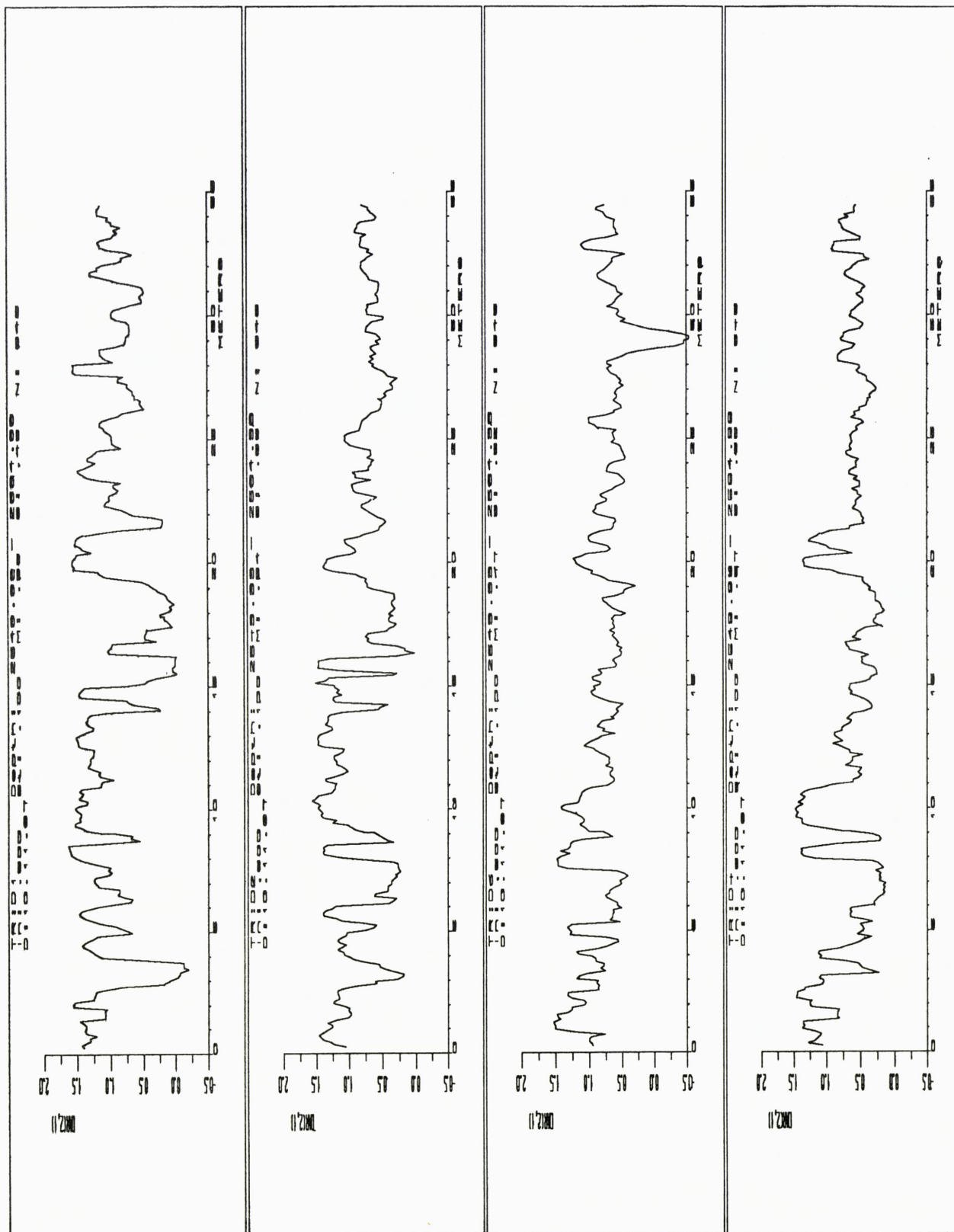


Fig. 2A

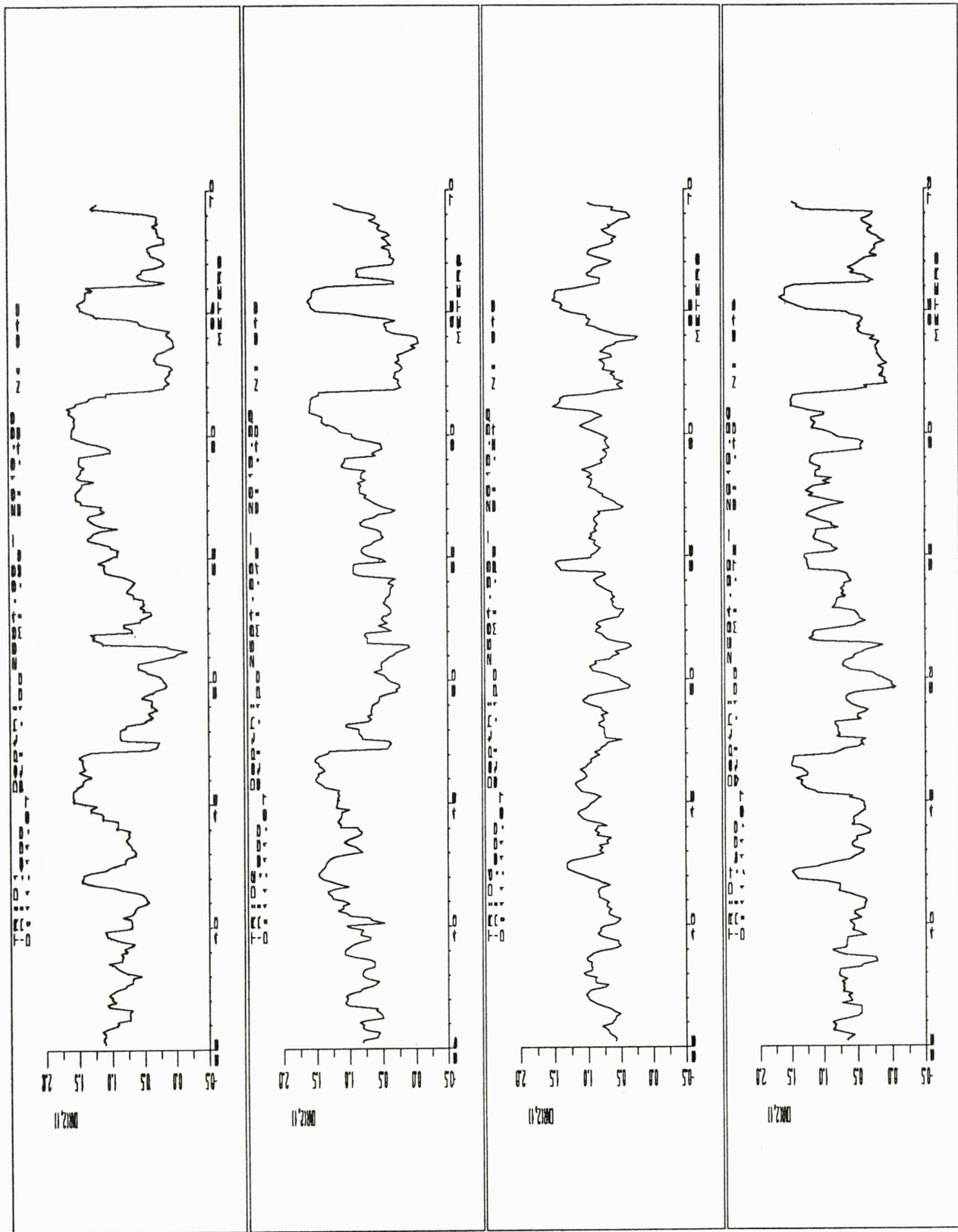


Fig. 2B

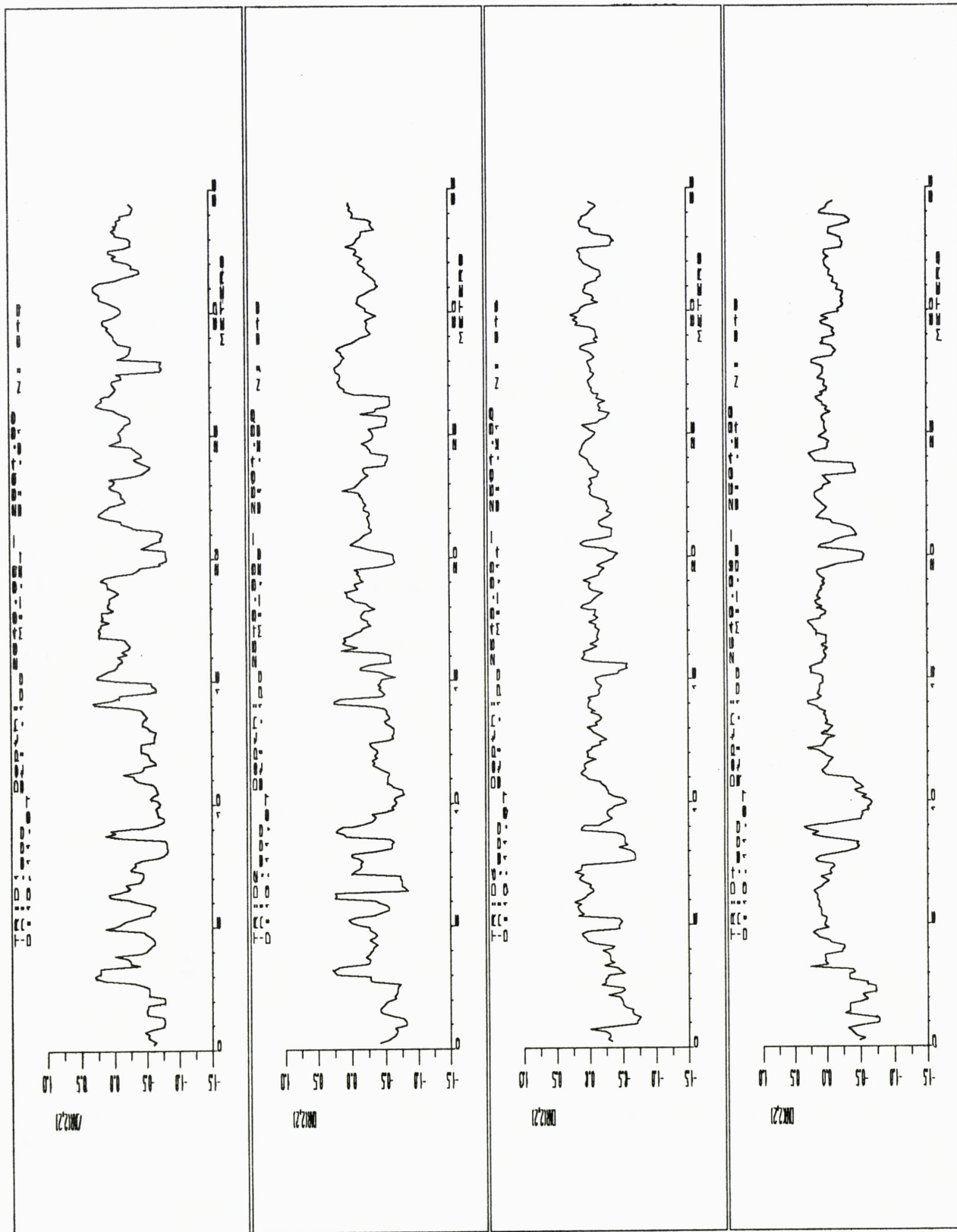


Fig. 3A

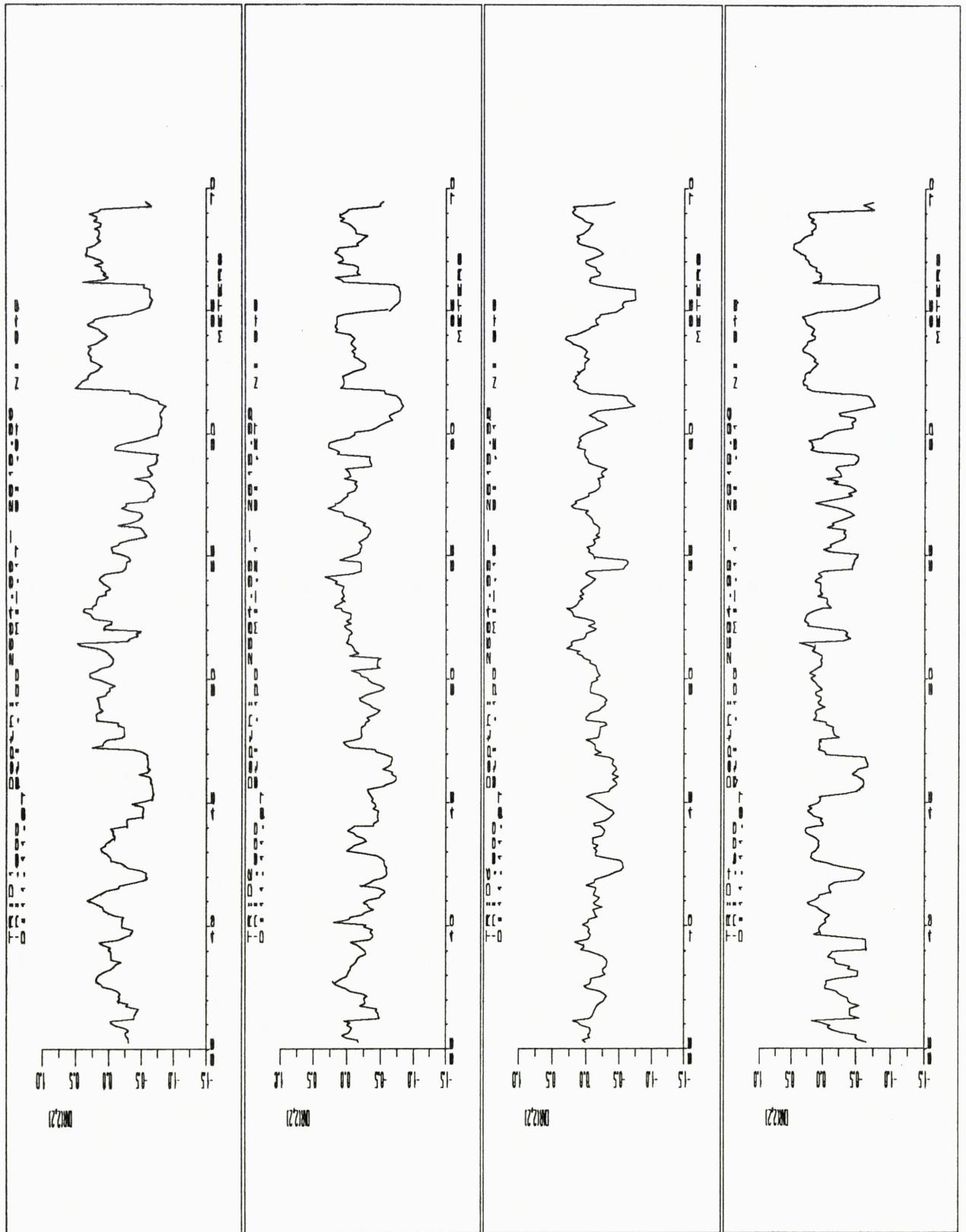


Fig. 3B

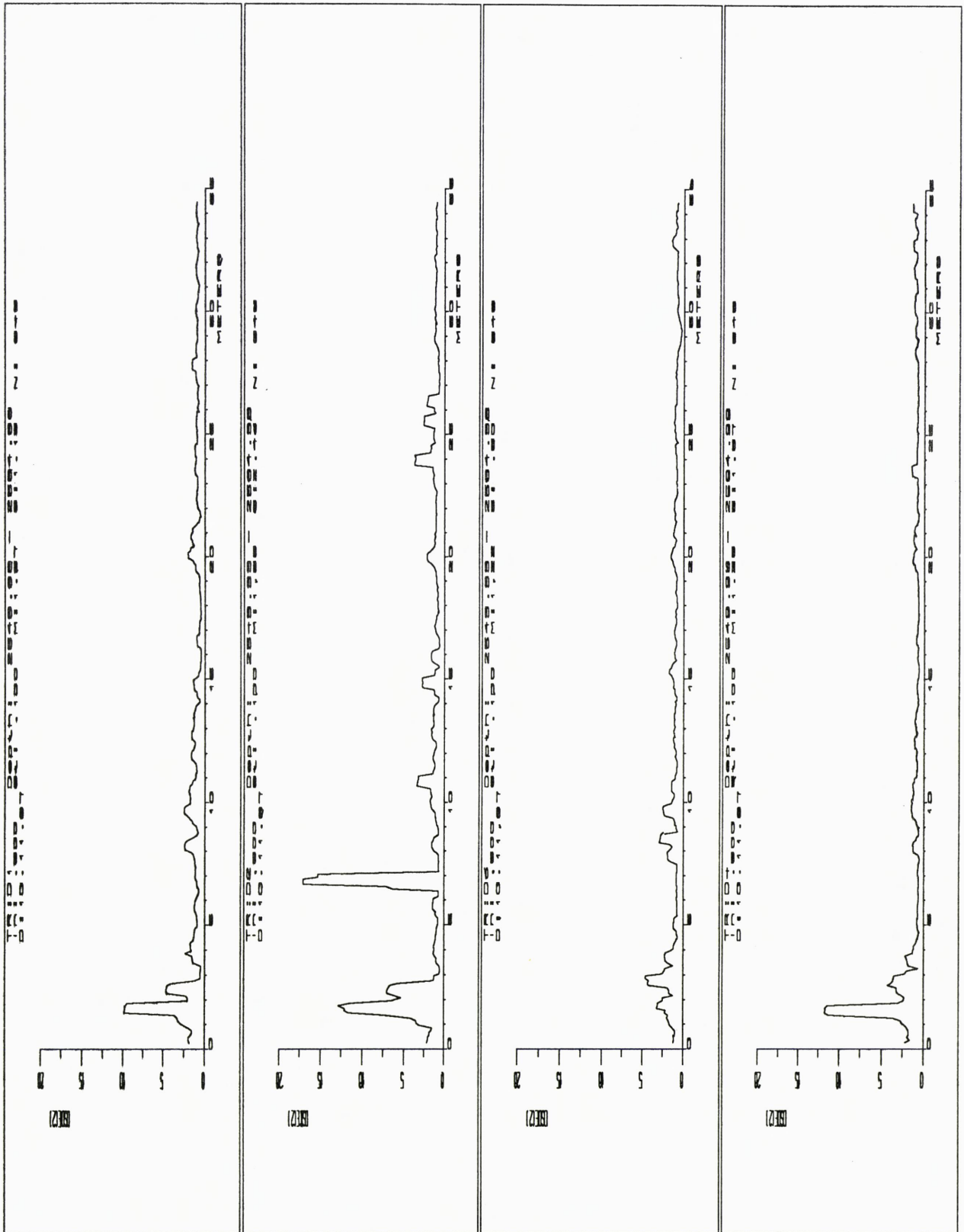


Fig. 4A

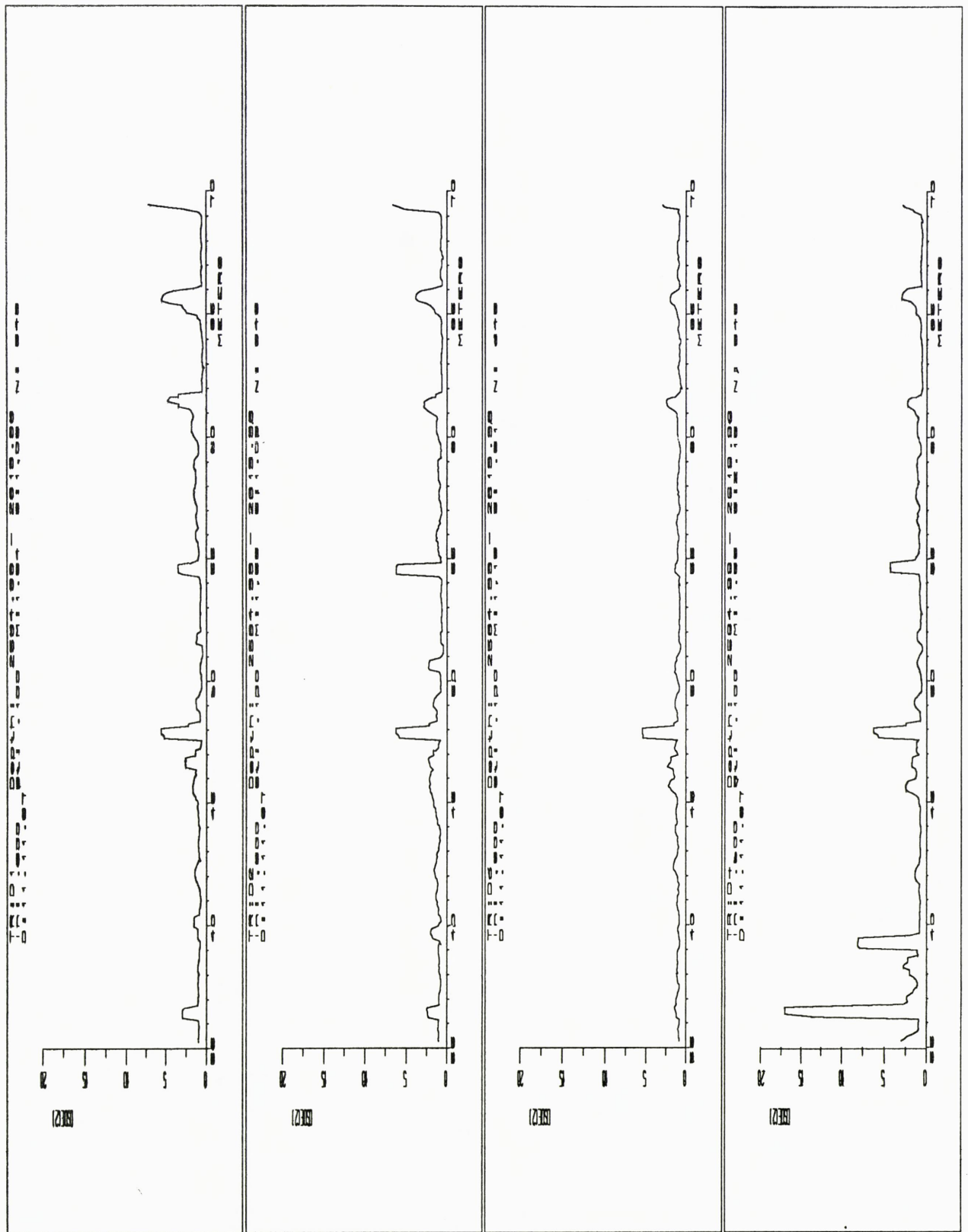

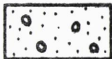
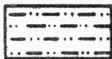



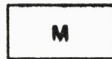
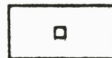
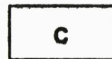
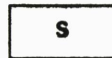


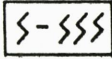


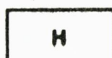

Fig. 4B

SYMBOL-LISTE

LITOLOGI

	SANDSTEIN
	SANDSTEIN, GRUSHOLDIG
	SILTSTEIN,
	SKIFER
	KULL
	SEMENT, KALSITT
	GLIMMER
	PYRITT
	KULLFRAGMENTER/ ORGANISK MATERIALE
	SIDERITT

ANDRE SYMBOL

	BIOTURBASJON, LITE - MYE
	SPOR ETTER PLANTERØTTER
	TREFRAGMENT
	HORIZONTAL
	VERTIKAL

PRIMÆRE SEDIMENTÆRE STRUKTURER

	LAGNING/LAMINASJON, HORIZONTAL
	LAGNING/LAMINASJON, HELLENDE, - FALL VIST
	KRYSSJIKTING
	RIFLER, SYMMETRISKE
	RIFLER, ASYMETRISKE
	BØLGEGENERERT STRUKTUR
	LAGNING/LAMINASJON; LINSET
	GRADERT LAGNING
	GRENSE; SKARP
	GRENSE: EROSIV
	GRENSE; GRADVIS

ANDRE STRUKTURER

	DEFORMERT STRUKTUR, «SLUMPING»
	MIKROFORKASTNING, FALL VIST

Fig. 5A

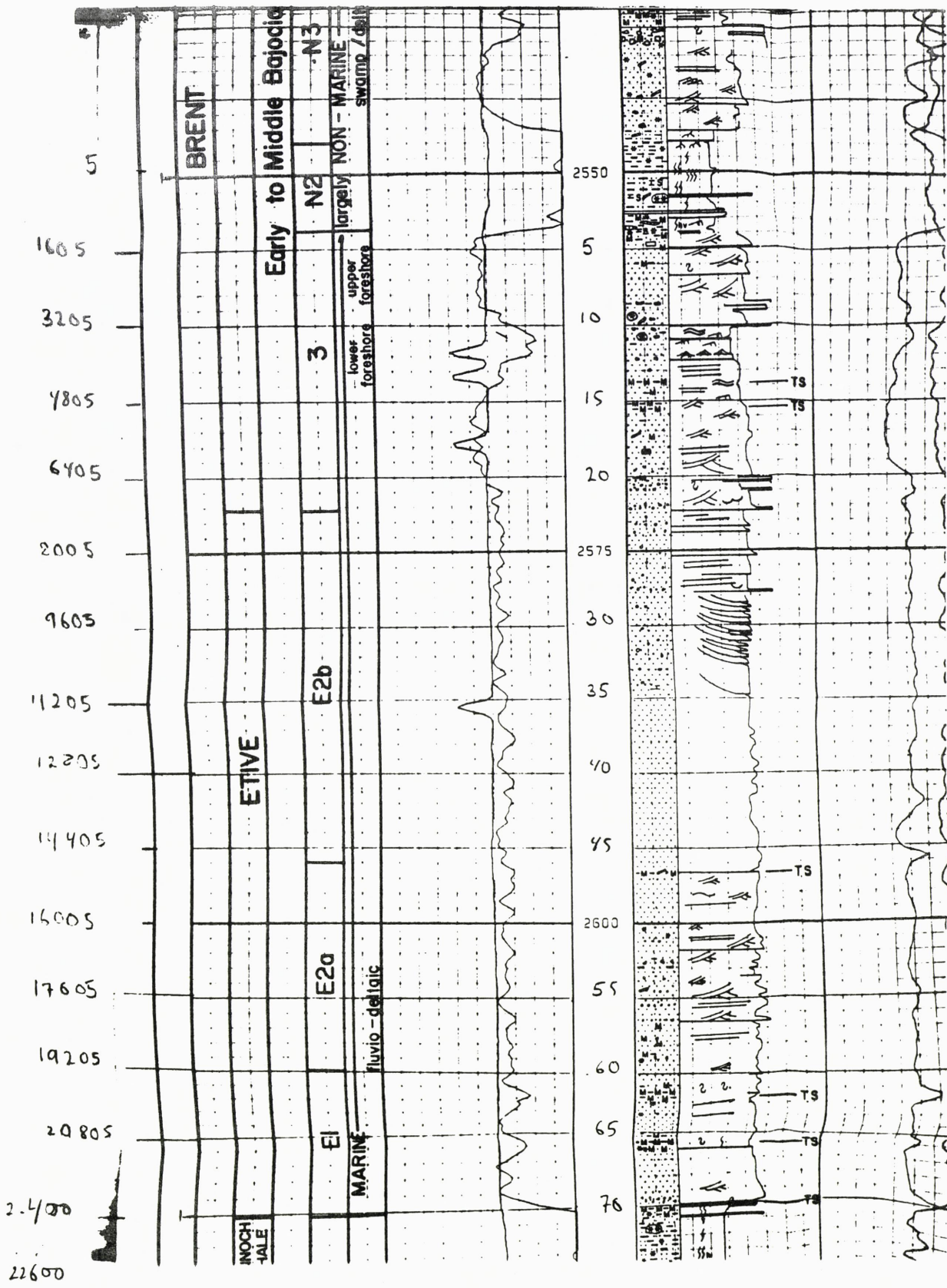


Fig. 5B

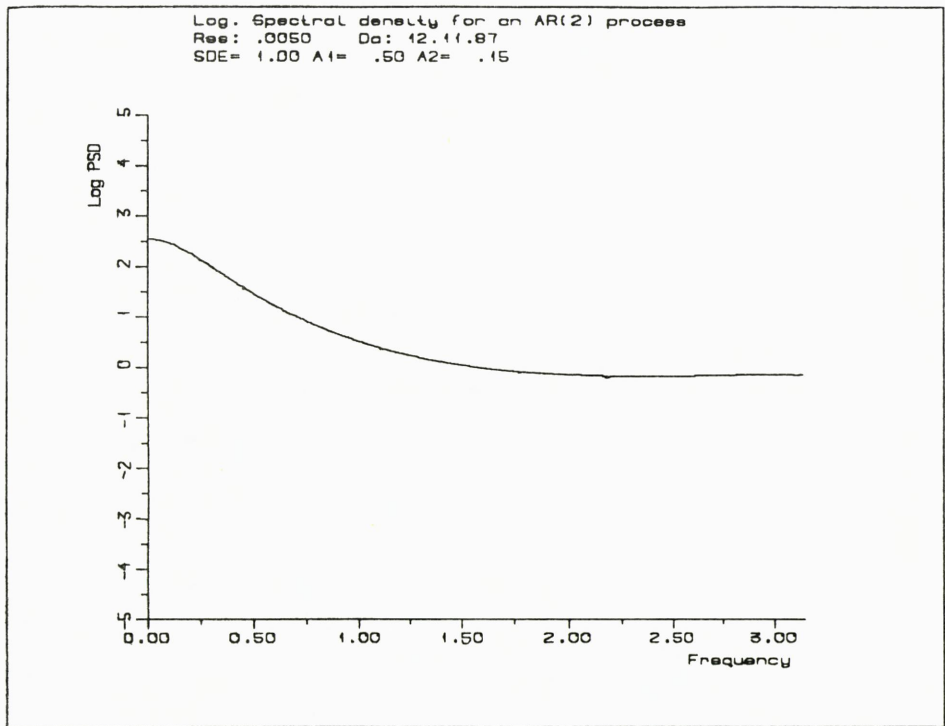
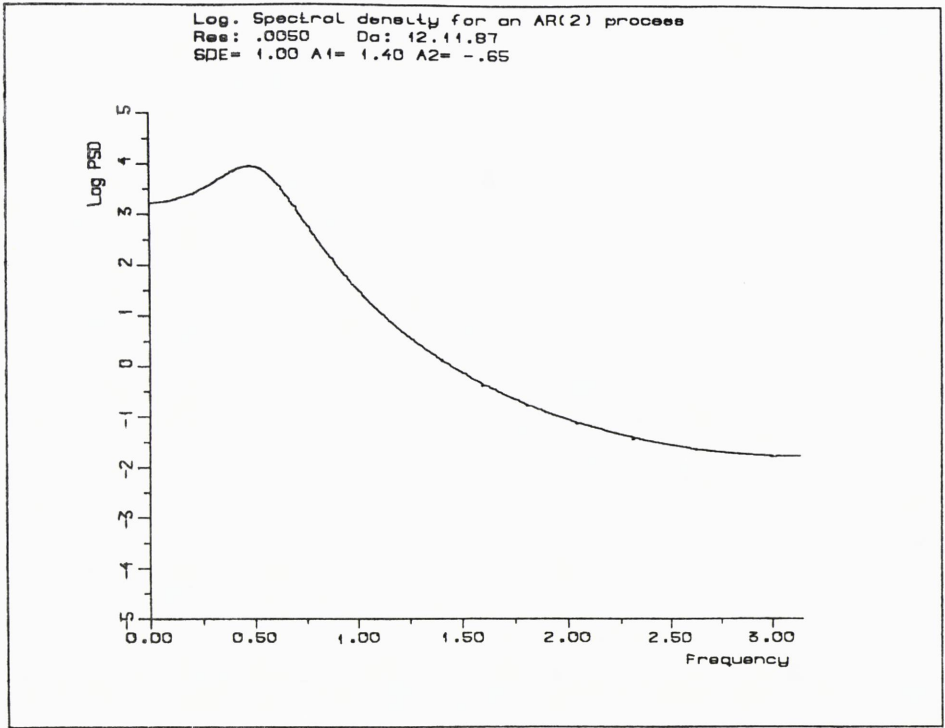


Fig. 6

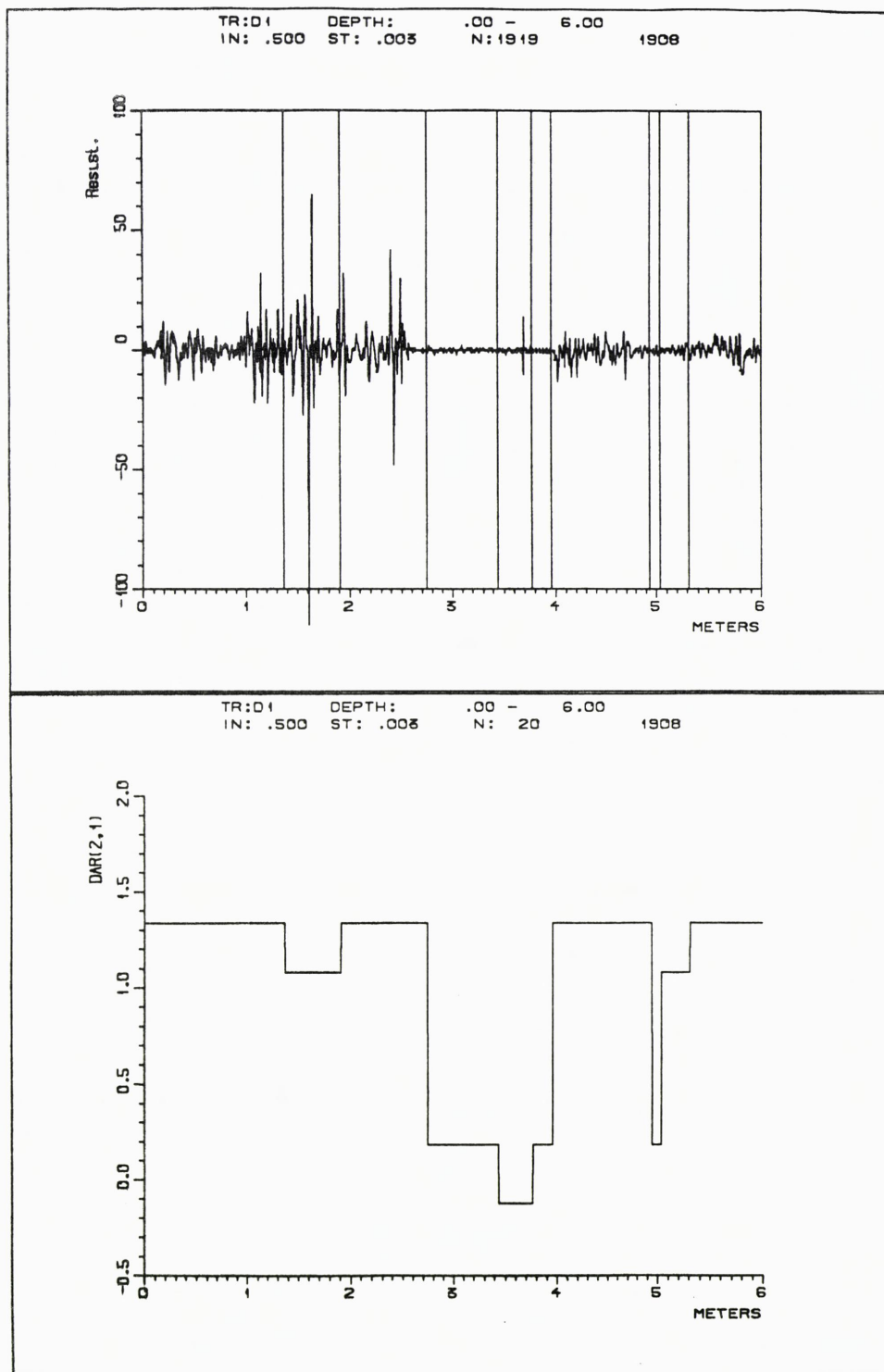


Fig. 7

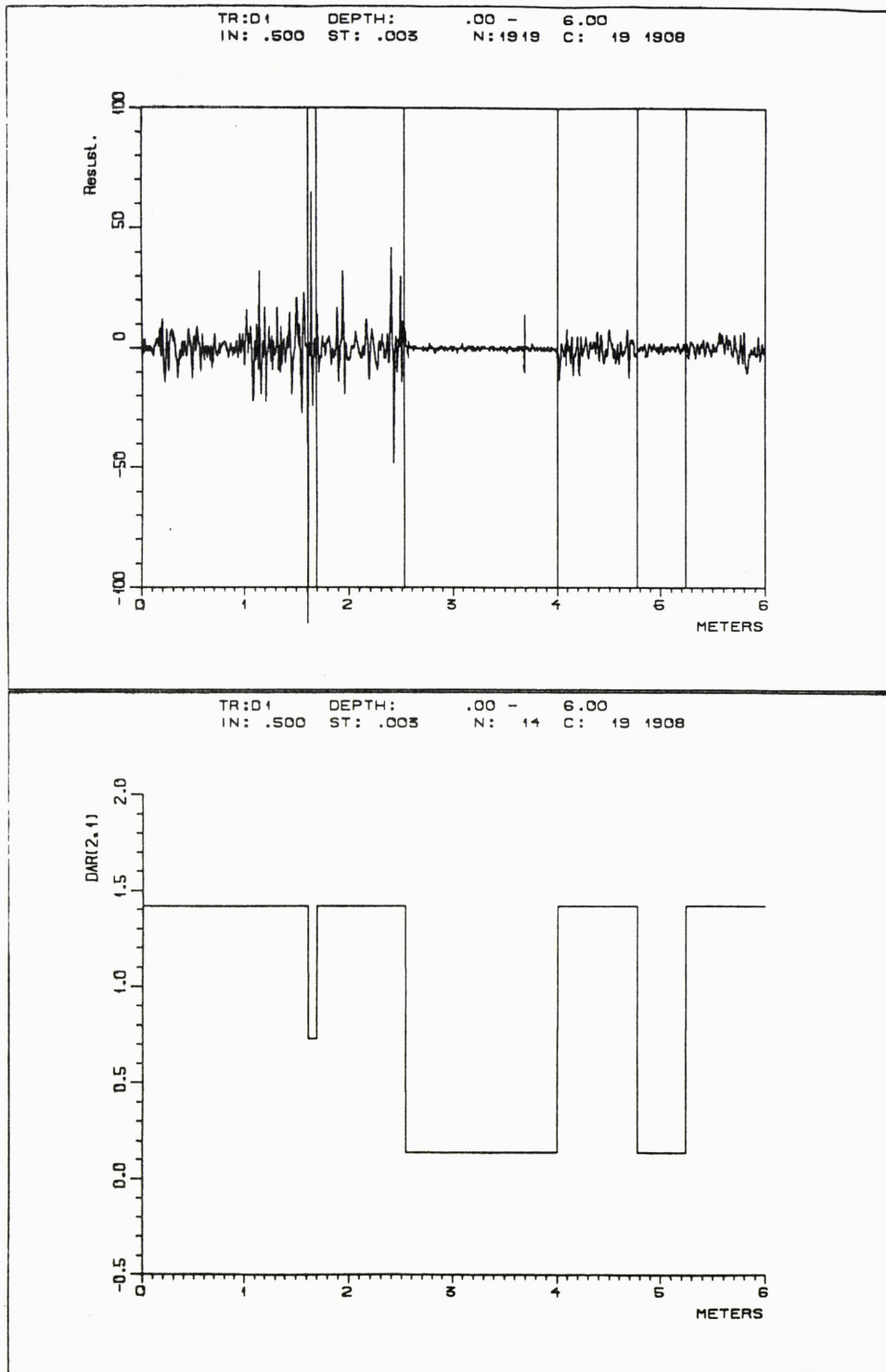


Fig. 8

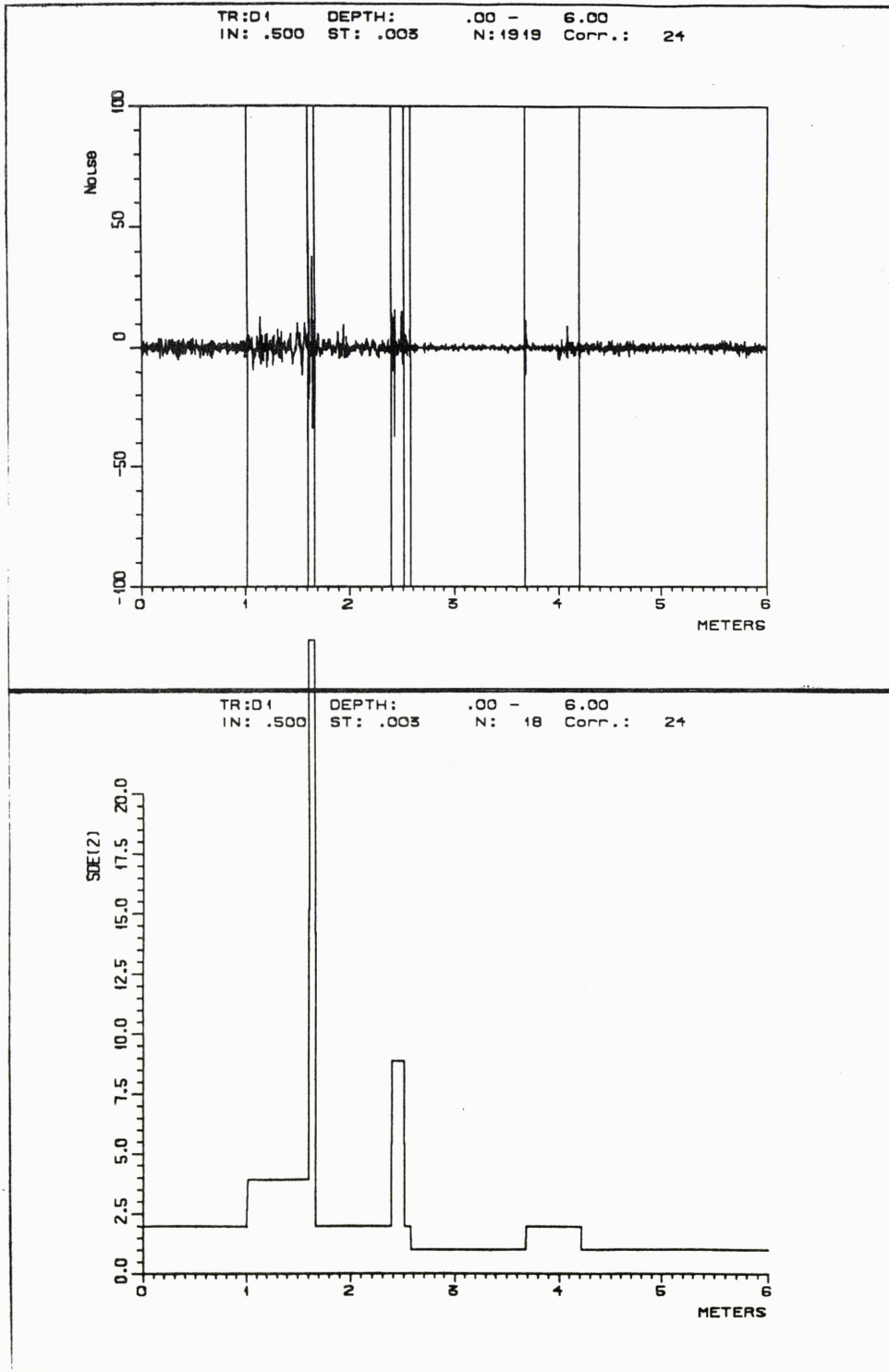


Fig. 9

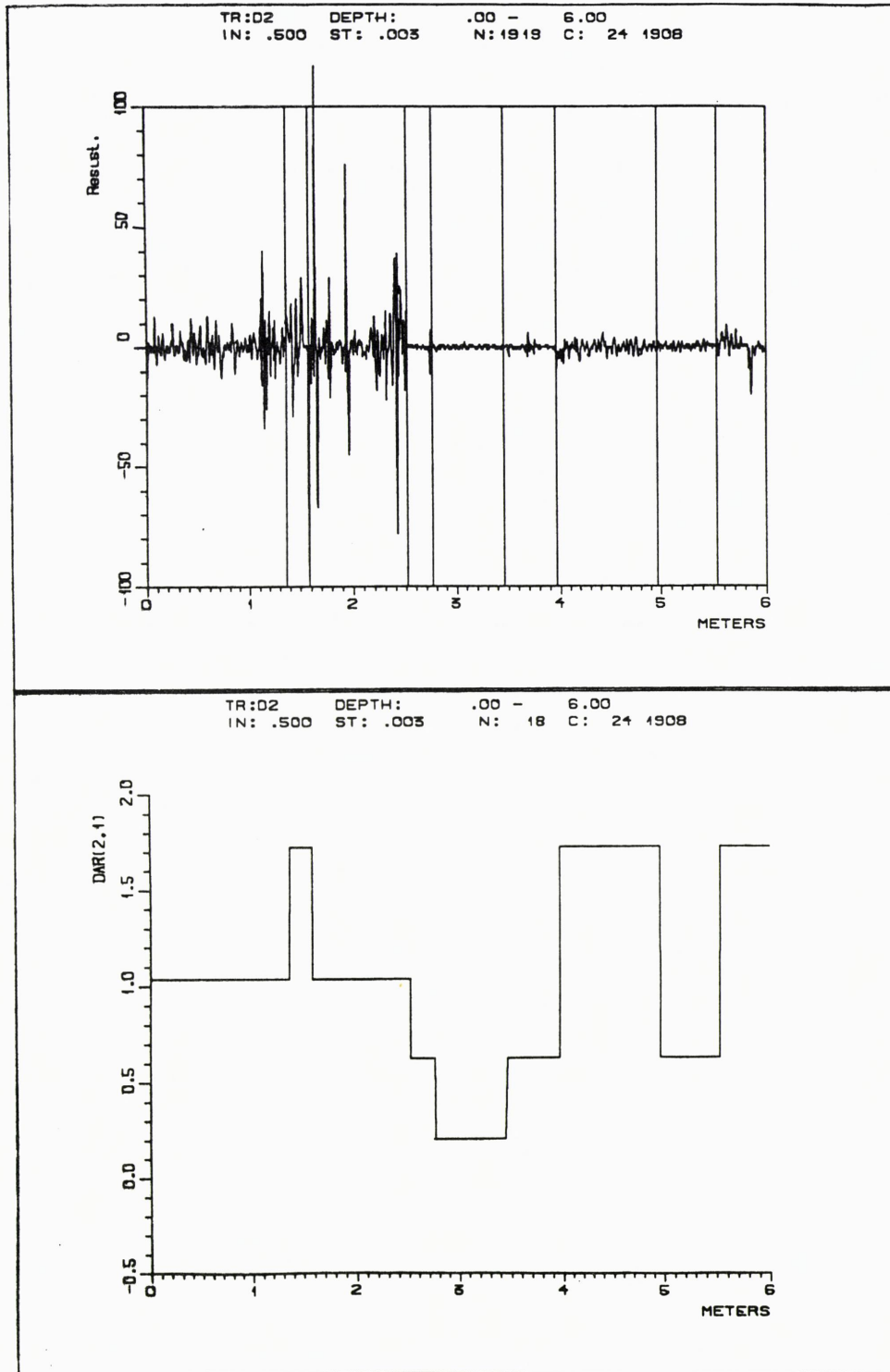


Fig. 10

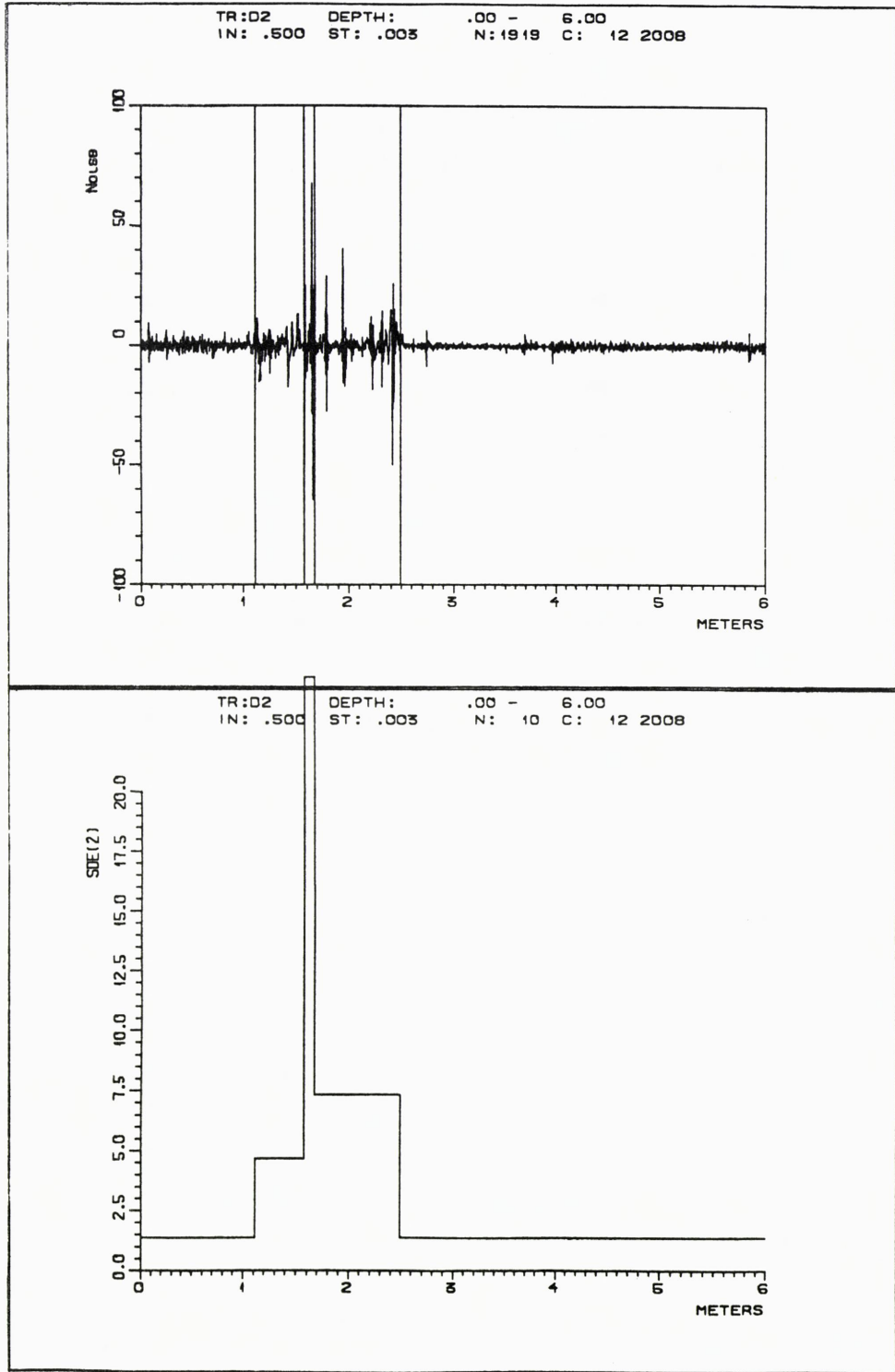


Fig. 11

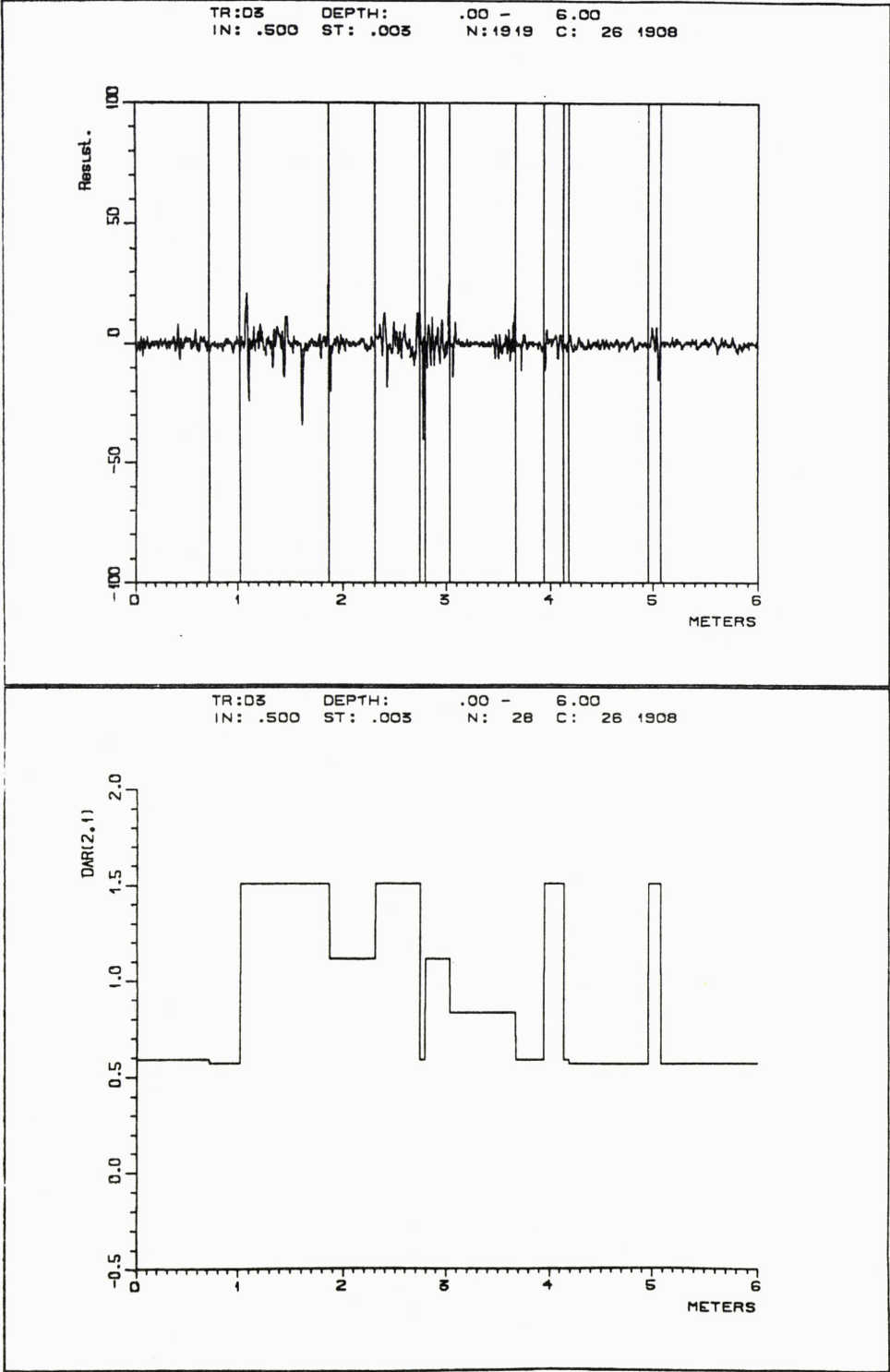


Fig. 12

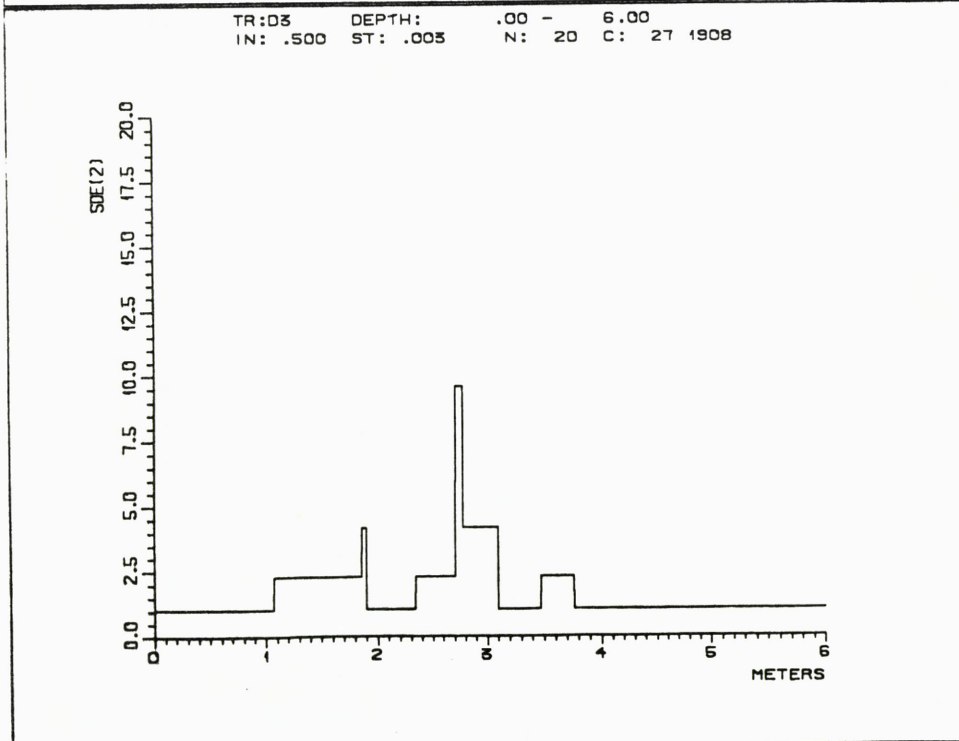
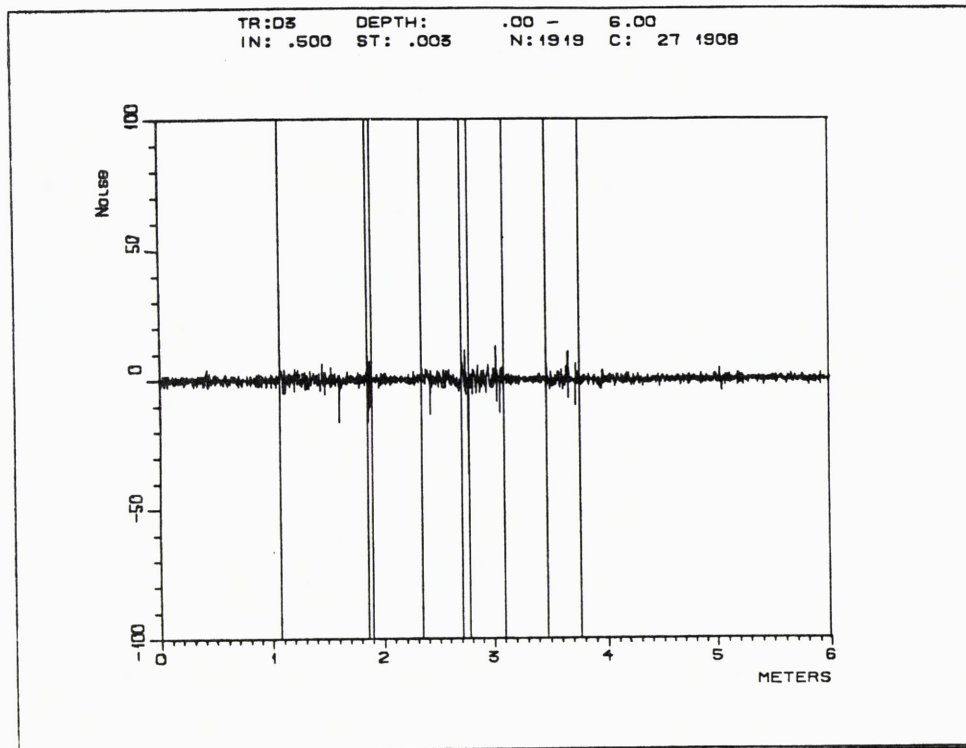


Fig. 13

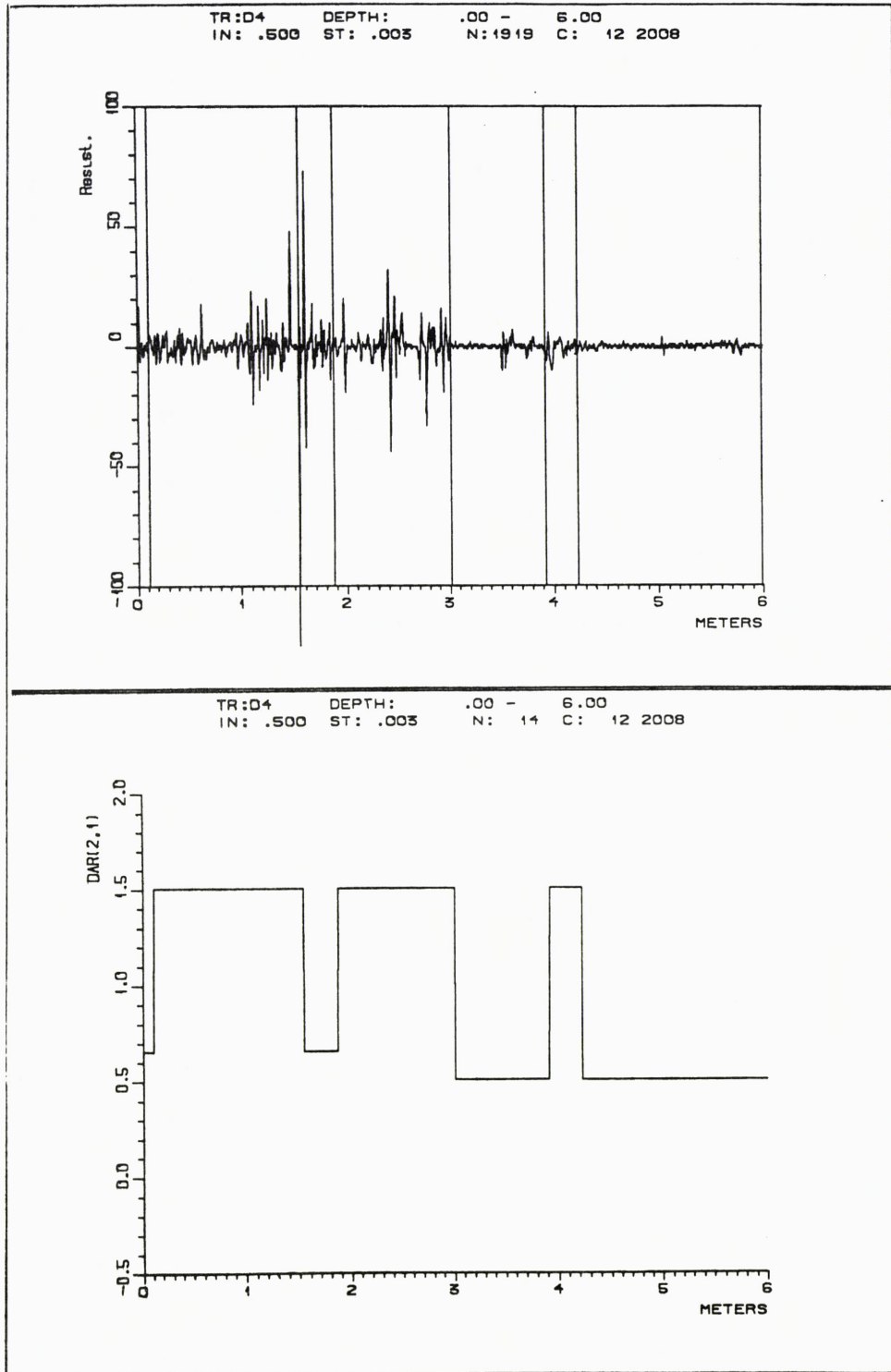


Fig. 14

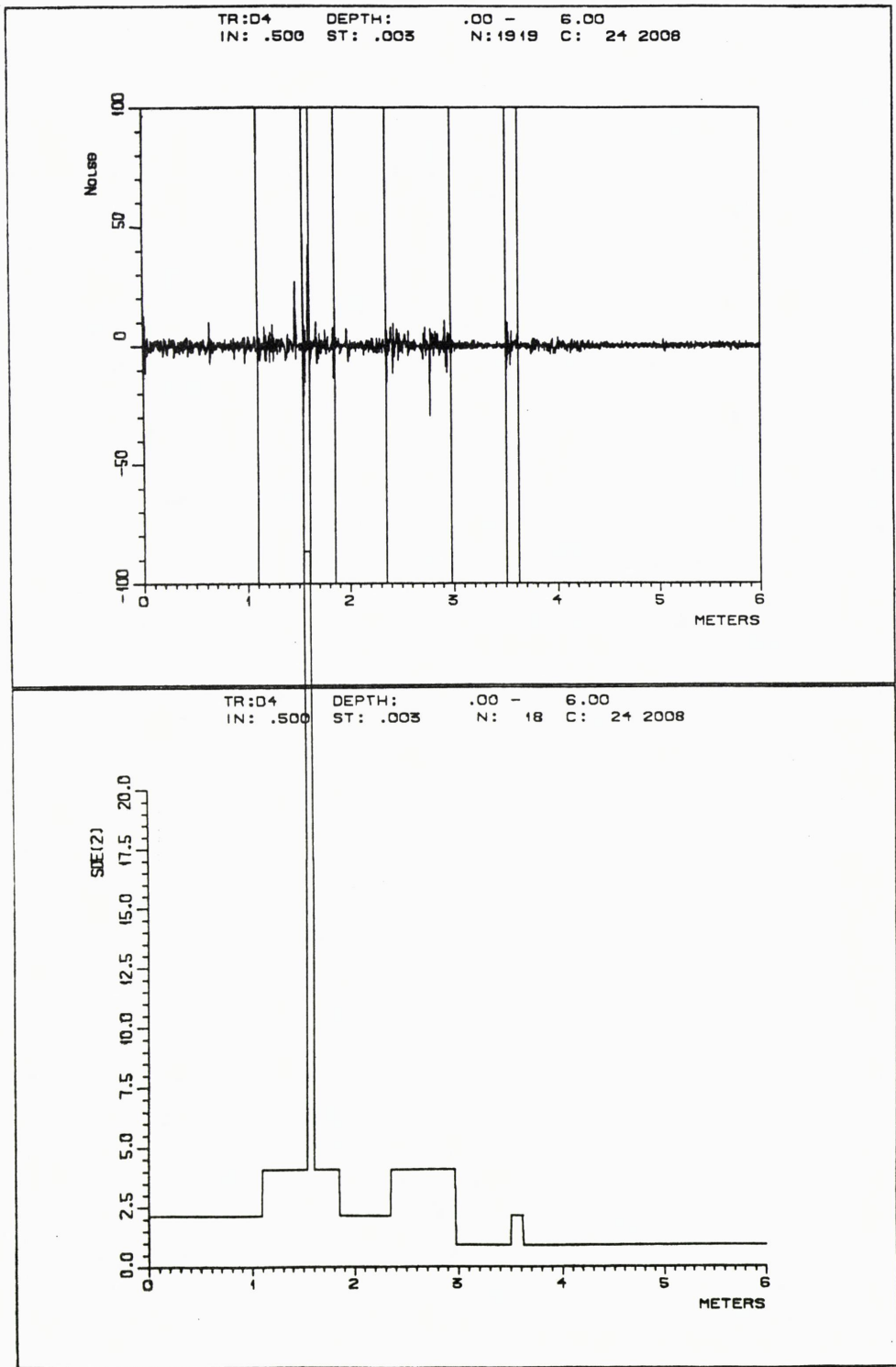


Fig. 15

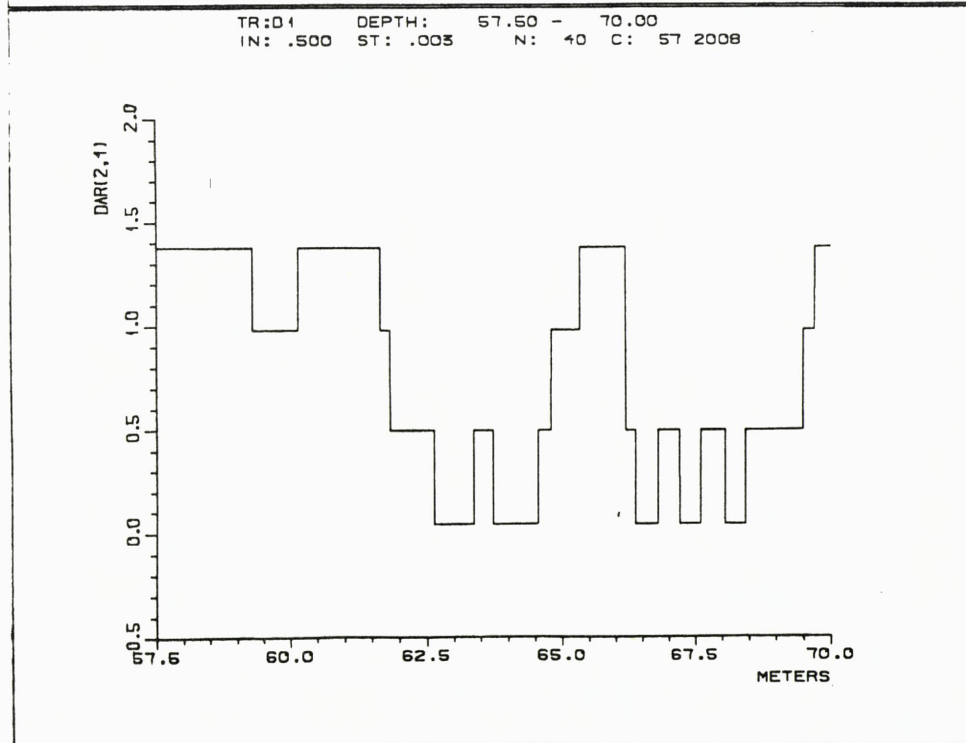
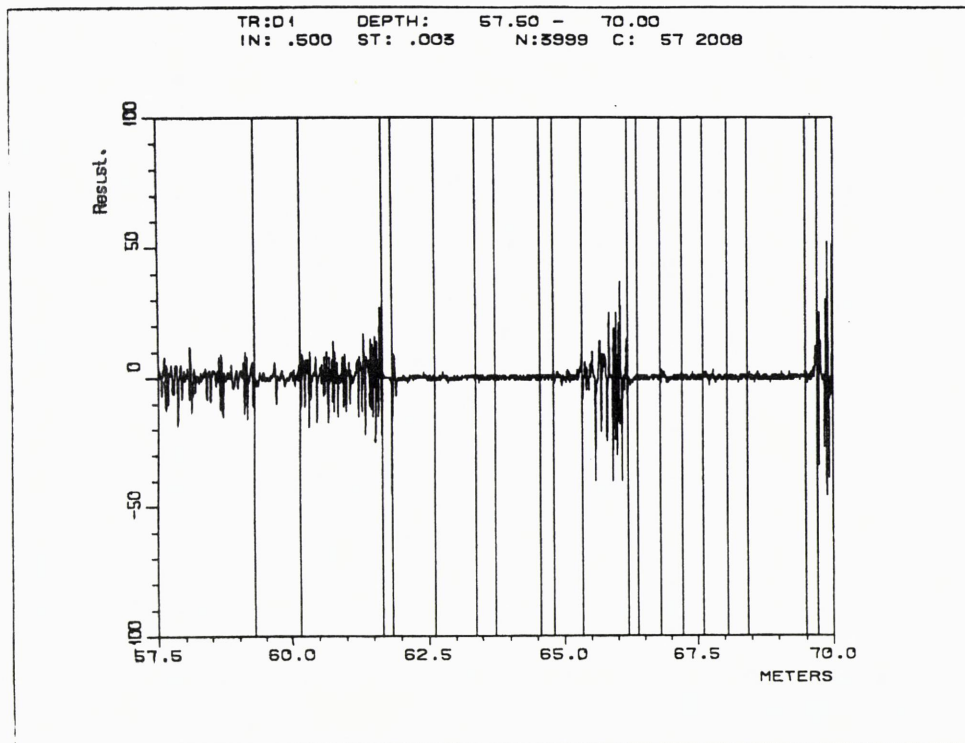


Fig. 16

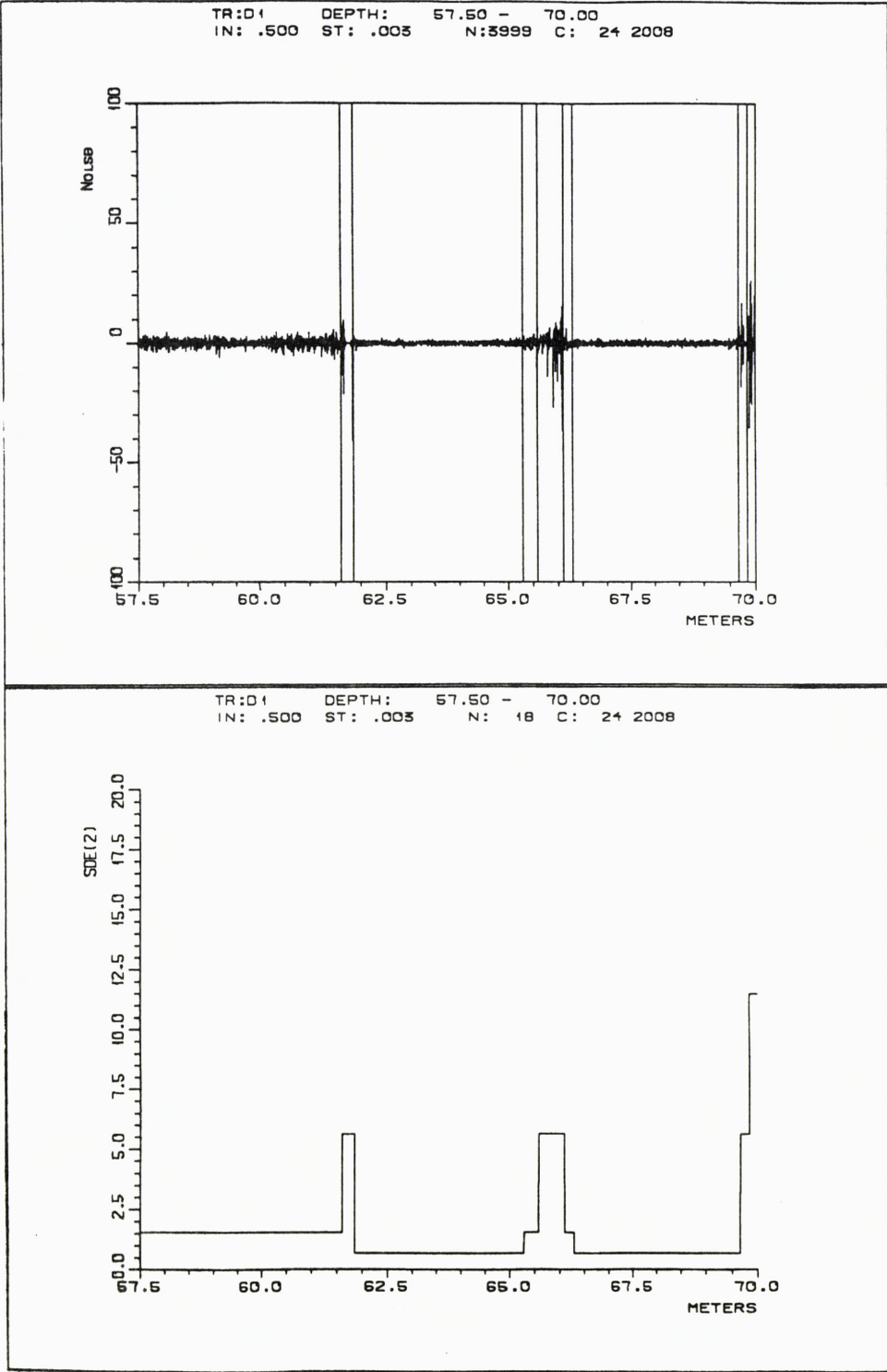


Fig. 17

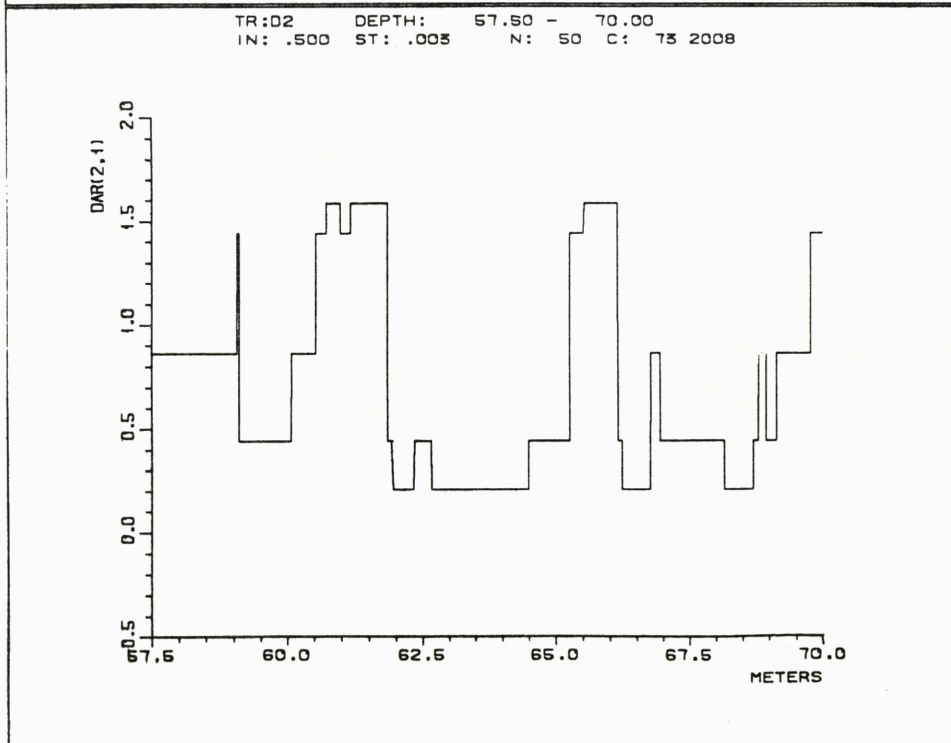
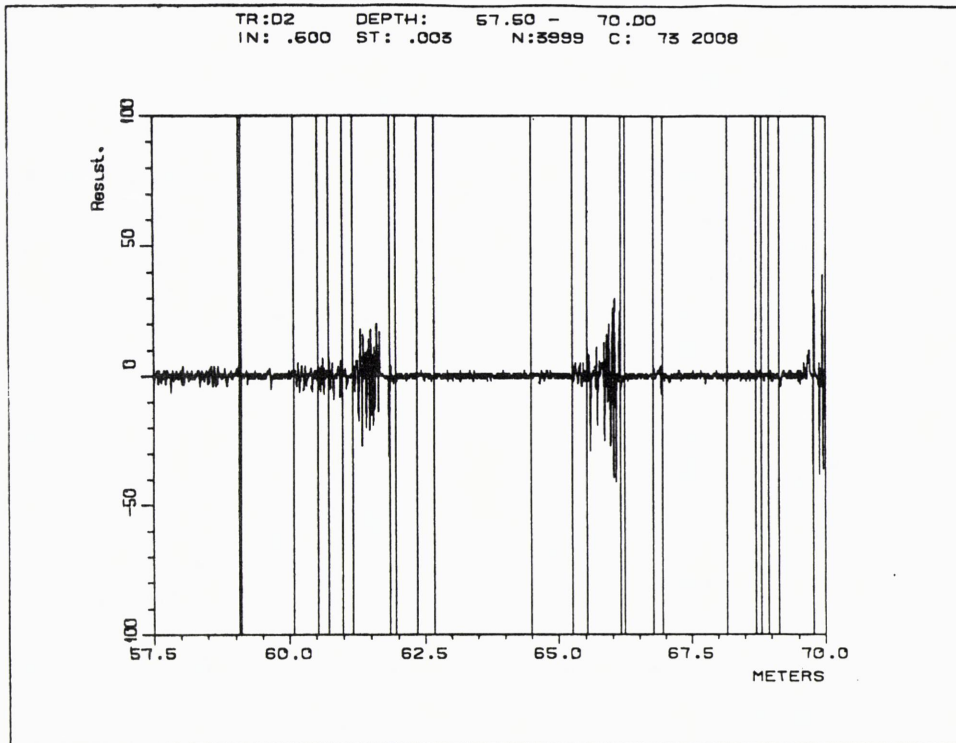


Fig. 18

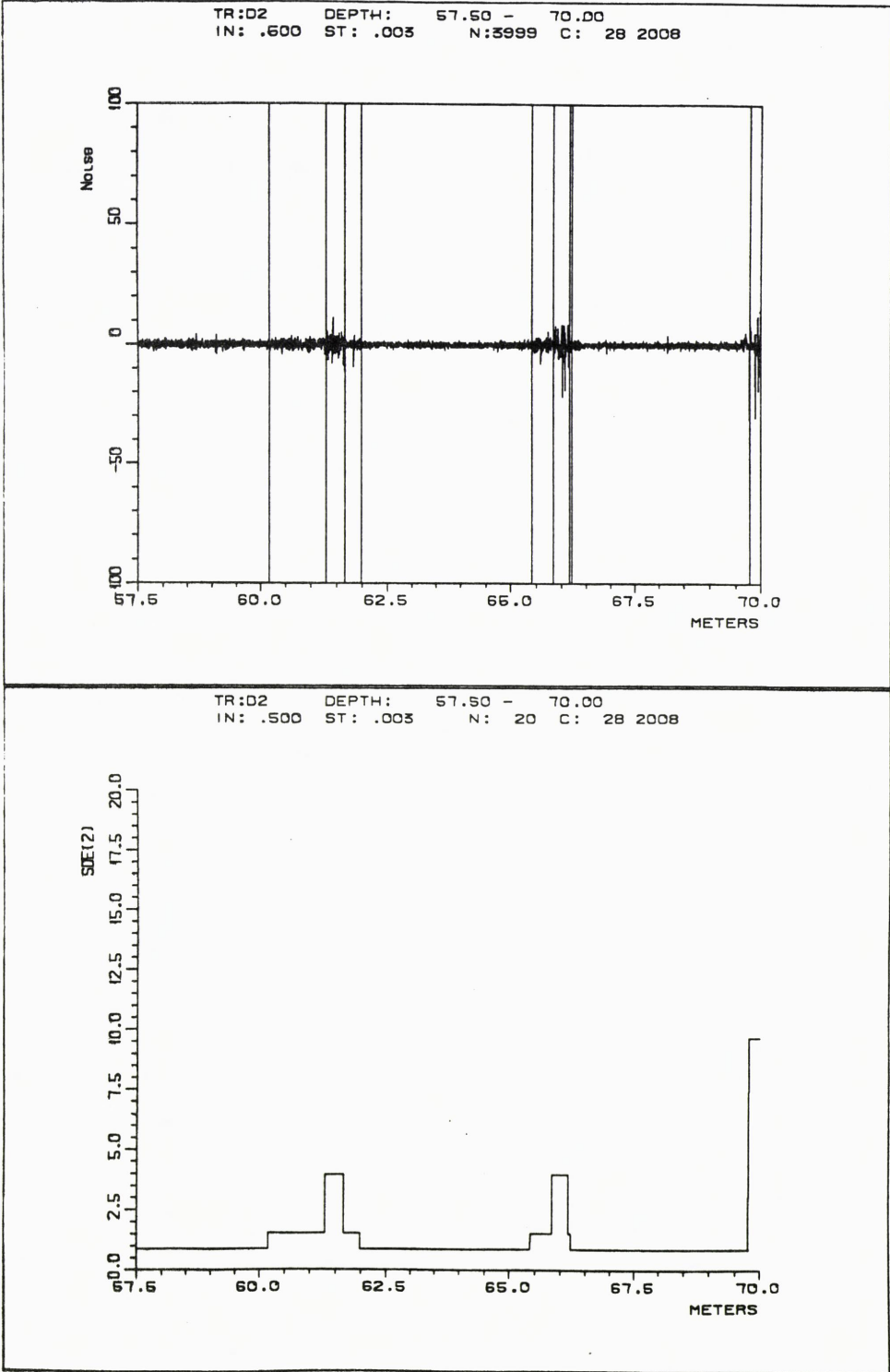


Fig. 19

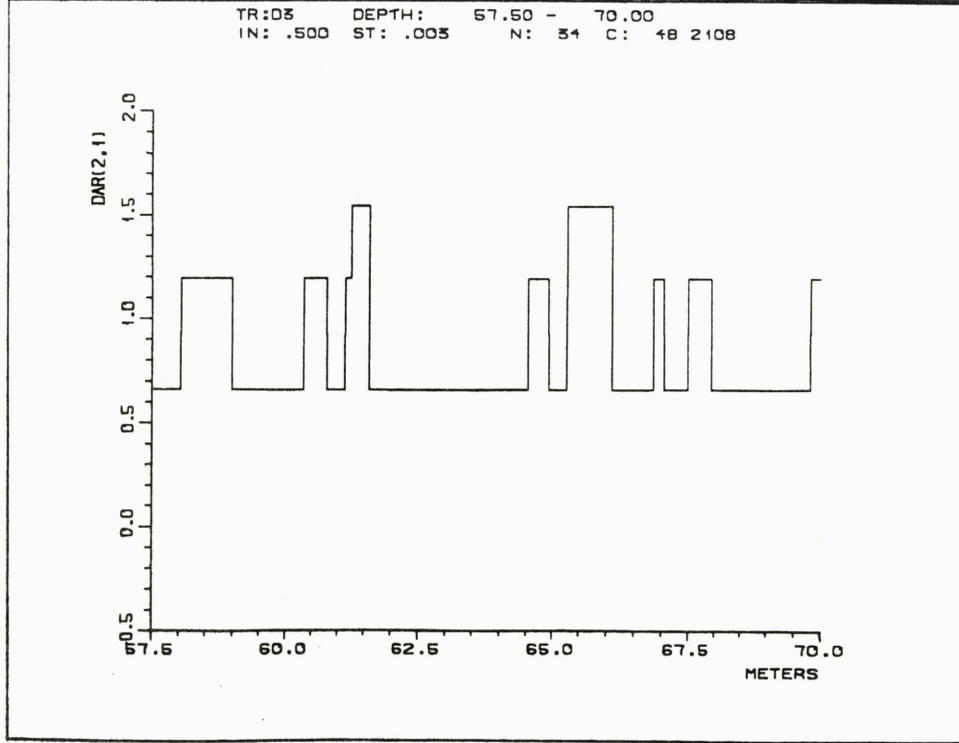
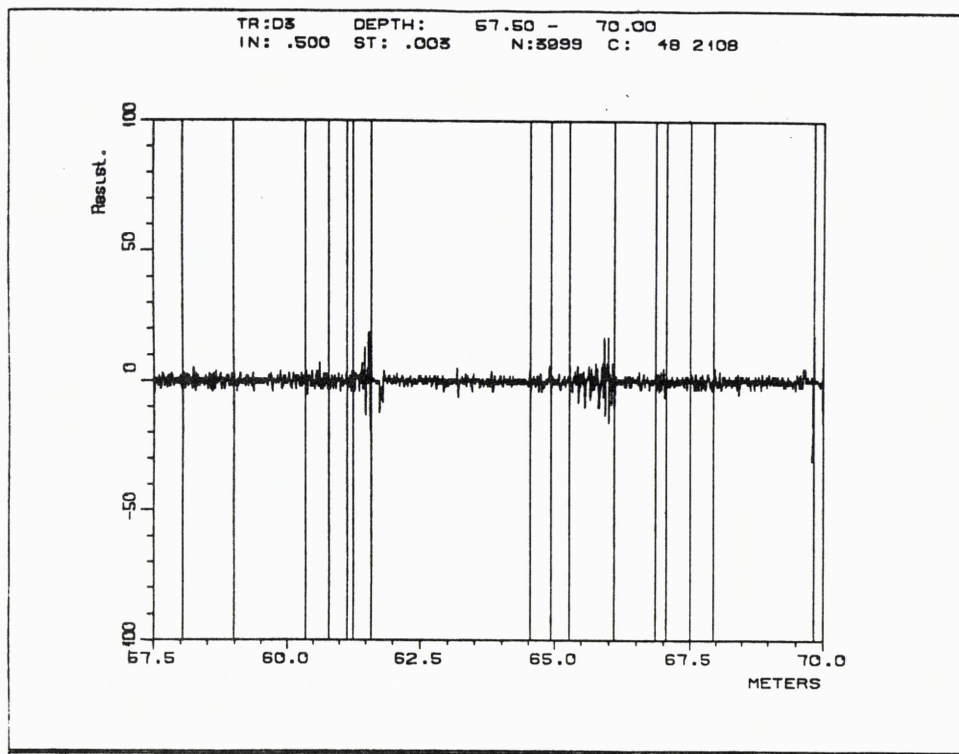


Fig. 20

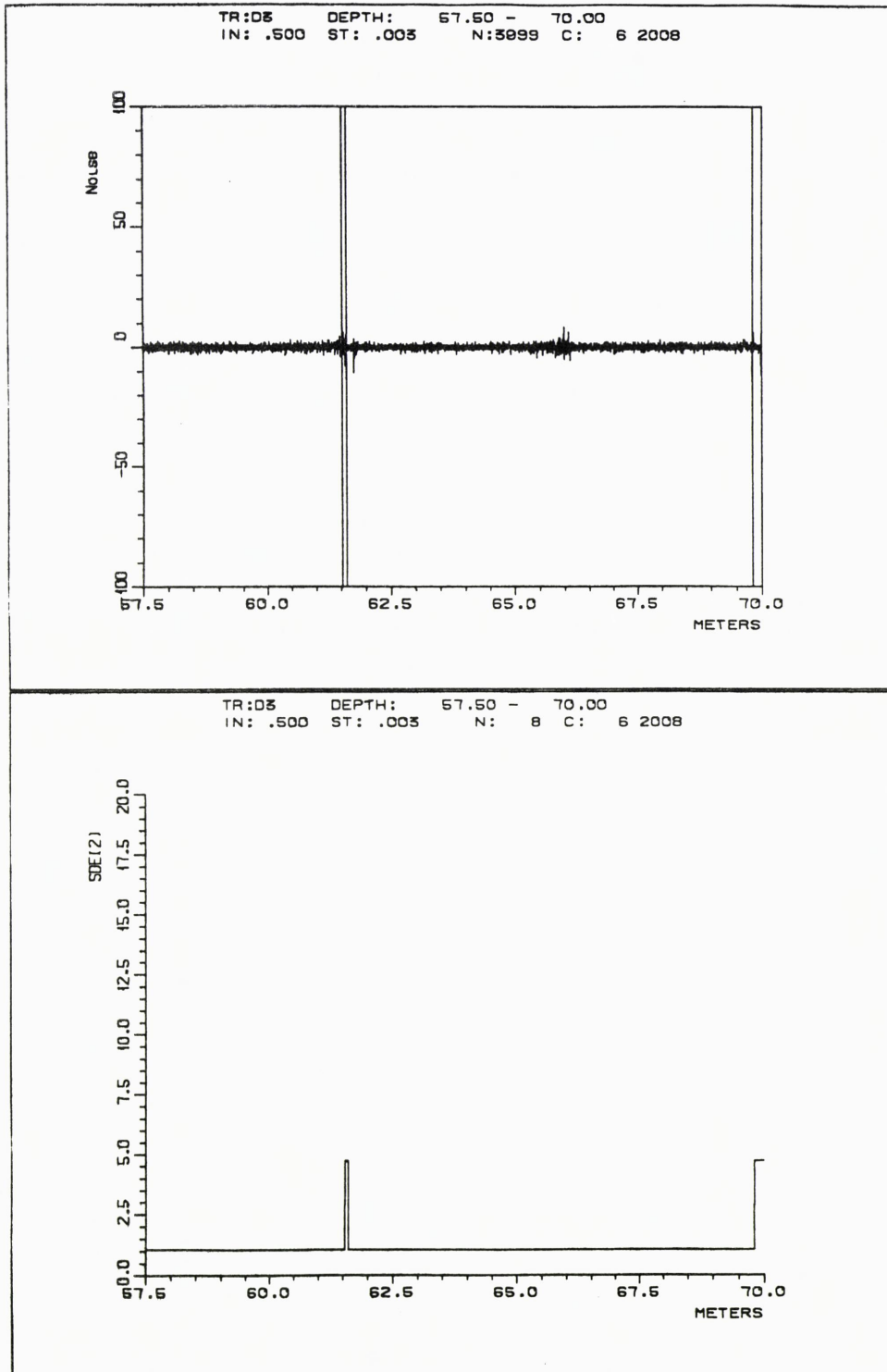


Fig. 21

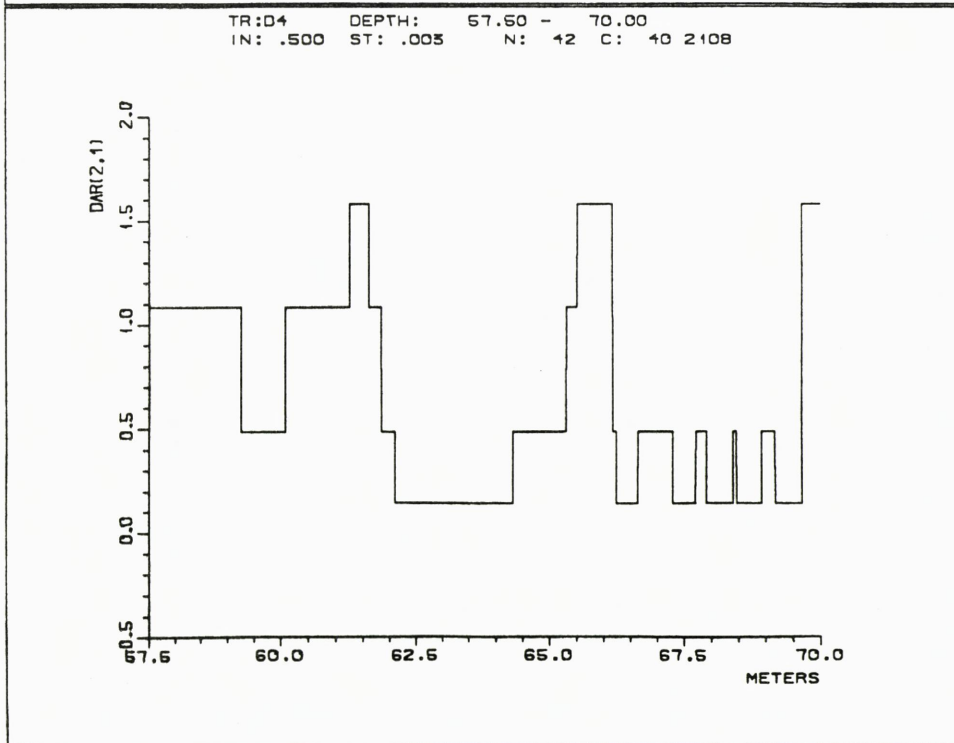
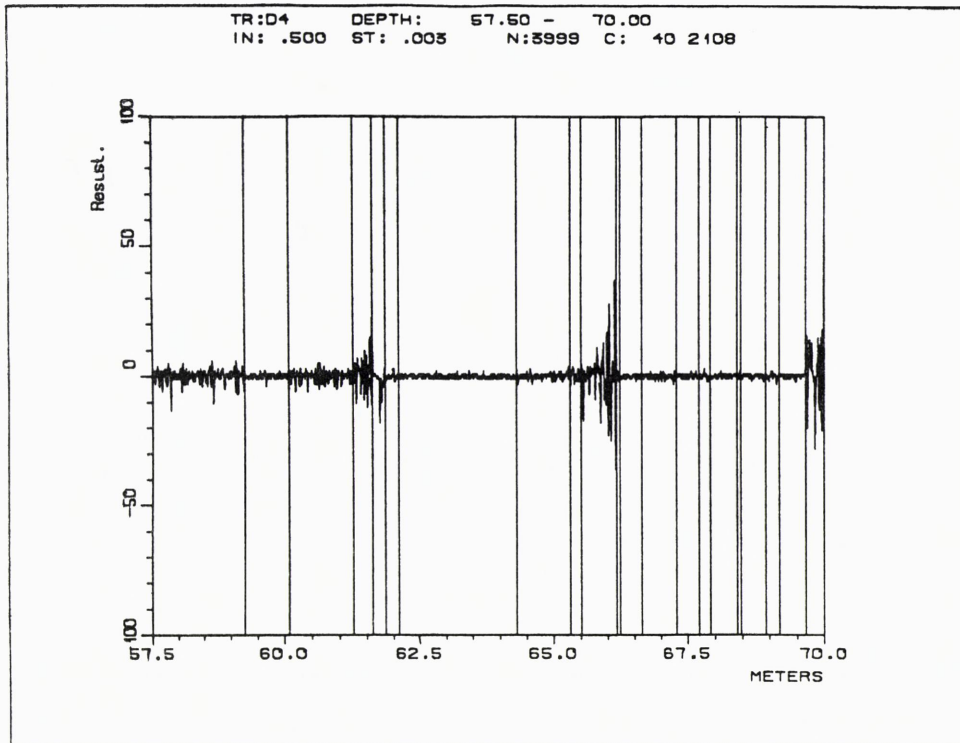


Fig. 22

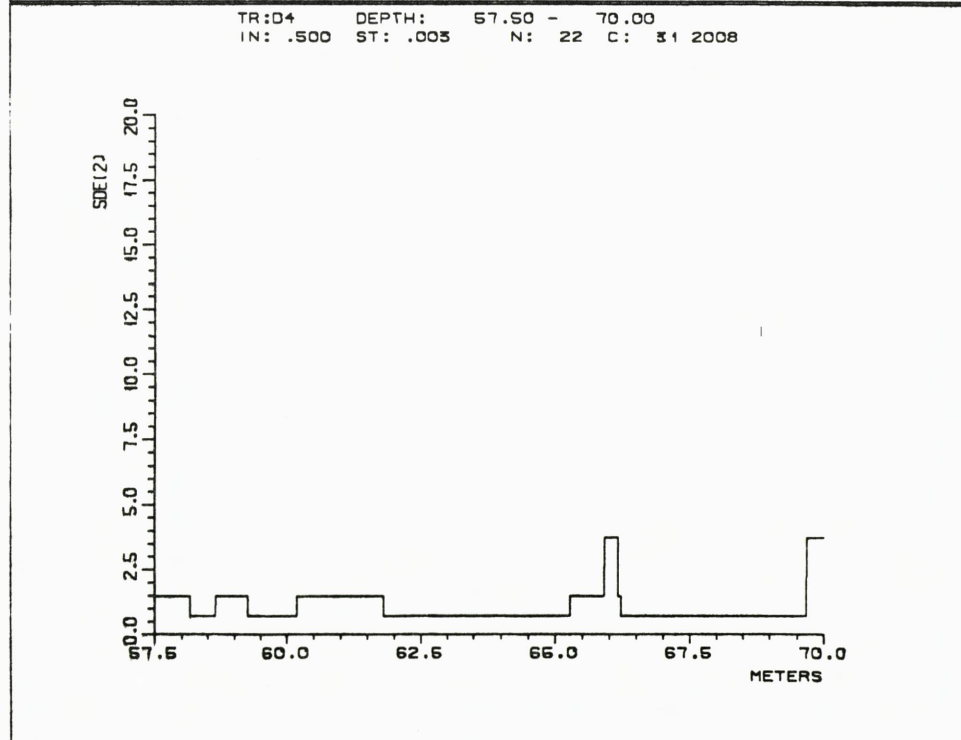
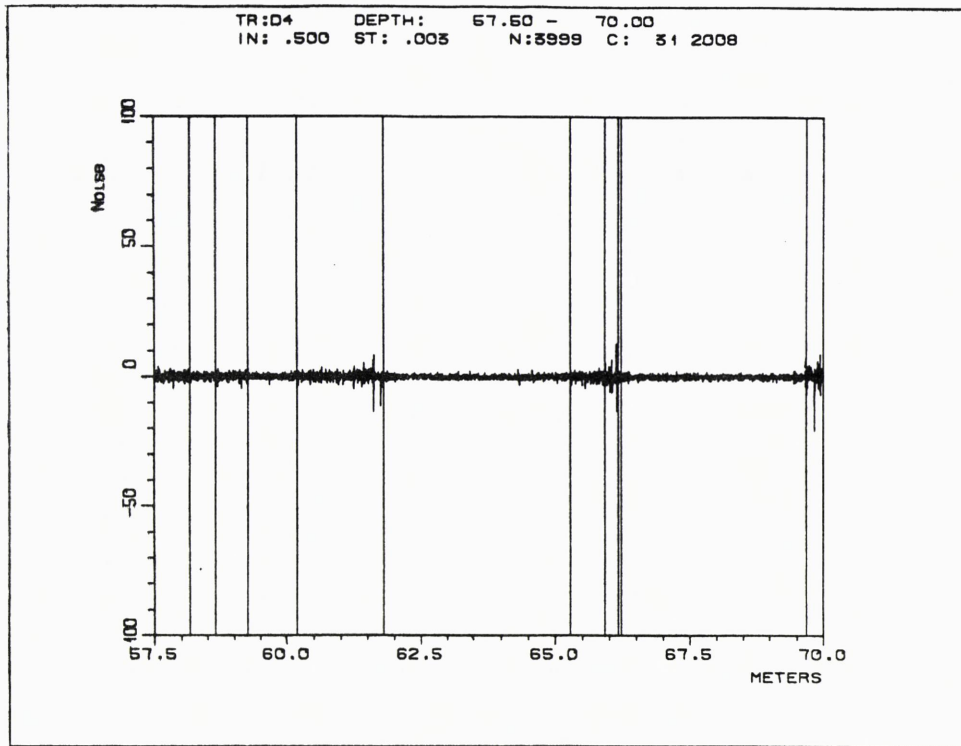


Fig. 23

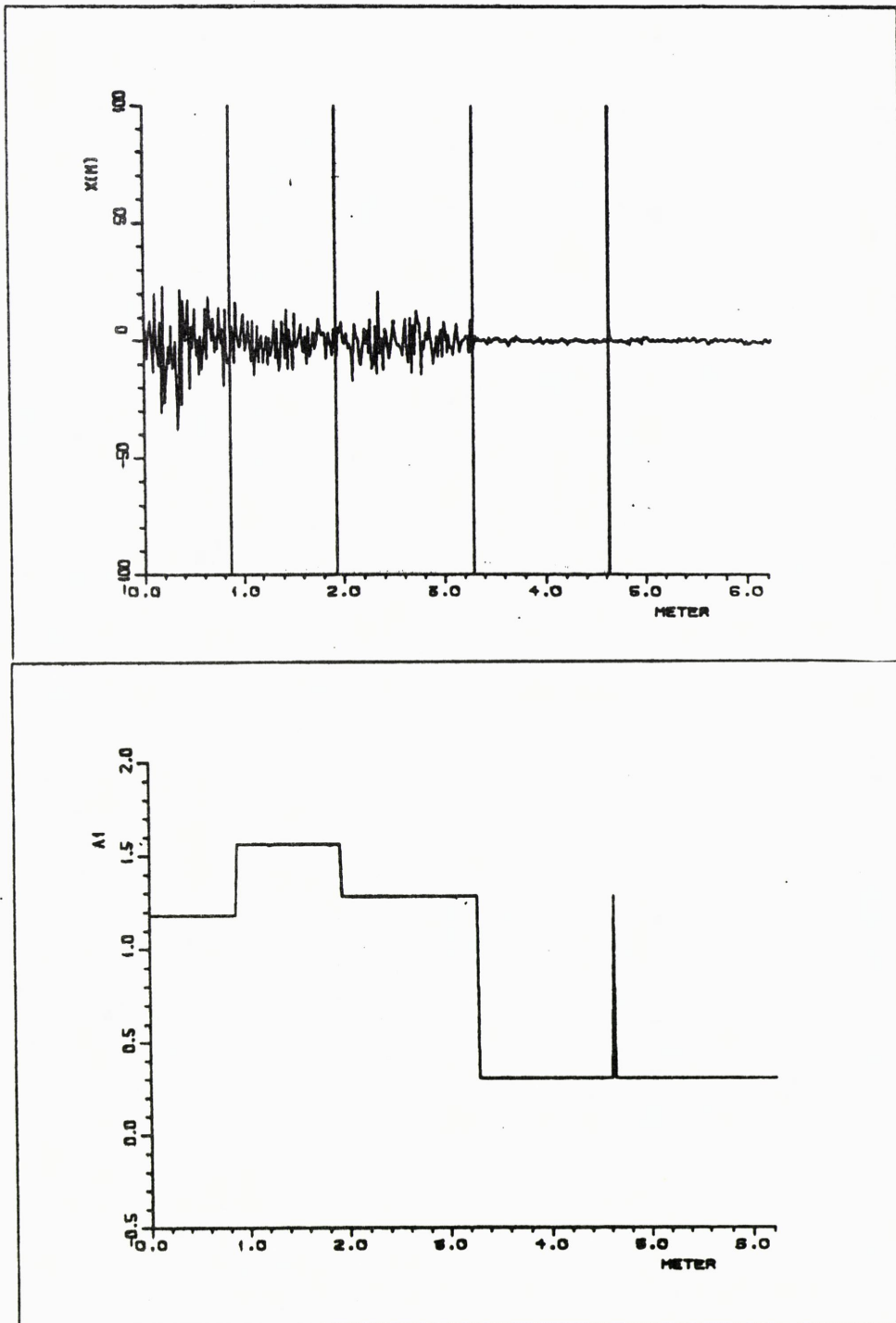


Fig. 24 a

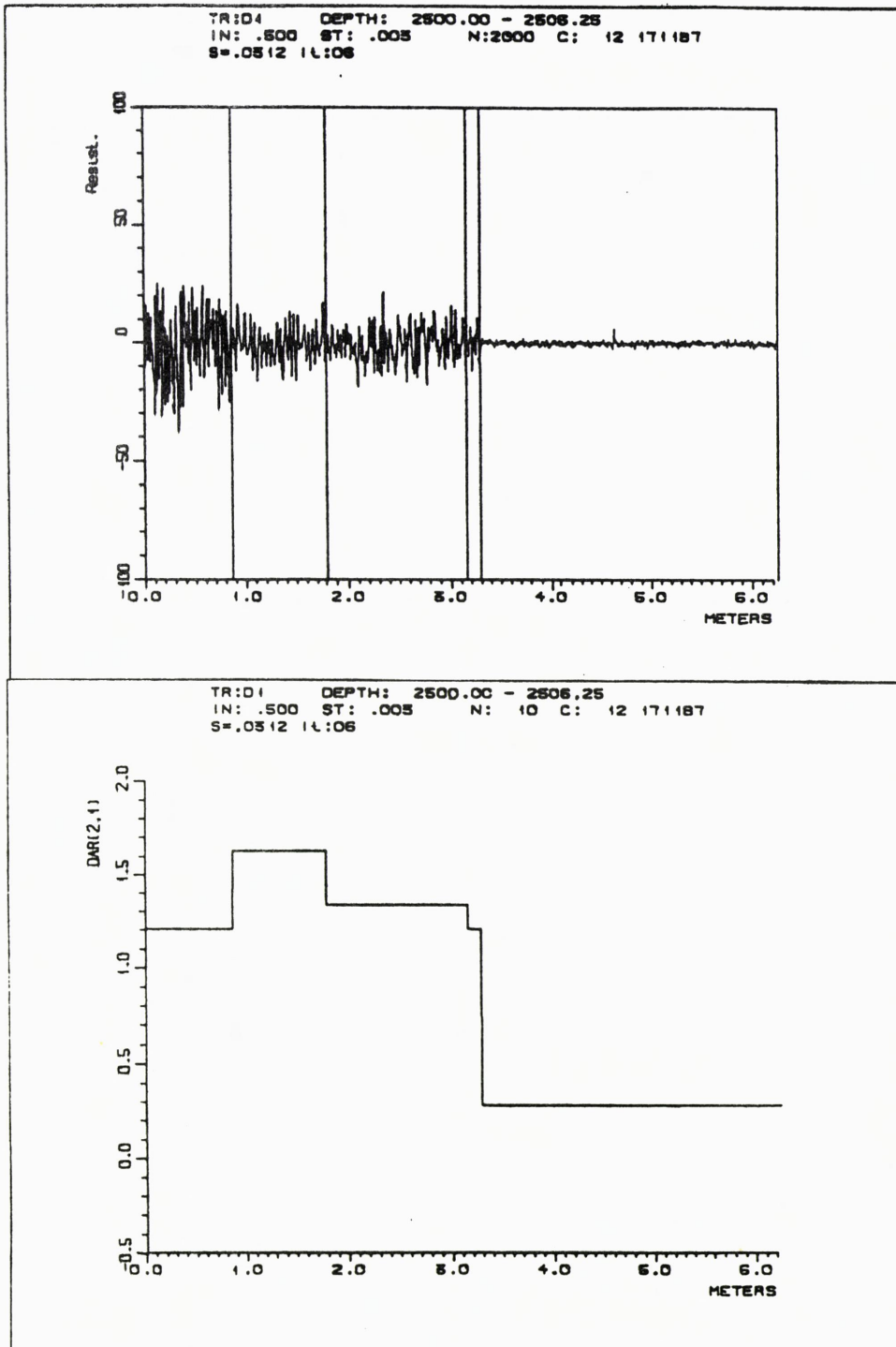


Fig. 24 b





Depotbiblioteket



76g0 83 640

